JOURNAL OF GEOPHYSICAL RESEARCH, VOL. 103, NO. D21, PAGES 28,265–28,289, NOVEMBER 20, 1998

MOZART, a global chemical transport model for ozone and related chemical tracers
1. Model description

G. P. Brasseur,[1] D. A. Hauglustaine,[1,2] S. Walters,[1] P. J. Rasch,[1]
J.-F. Müller,[3] C. Granier,[2,4,5] and X. X. Tie [1]

Abstract. We present a new global three-dimensional chemical-transport model (called MOZART) developed in the framework of the NCAR Community Climate Model (CCM) and aimed at studying the distribution and budget of tropospheric ozone and its precursors. The model, developed with a horizontal resolution of 2.8° in longitude and latitude, includes 25 levels in the vertical between the Earth's surface and an upper boundary located at approximately 35 km altitude. In its present configuration the model calculates the global distribution of 56 chemical constituents with a timestep of 20 min, and accounts for surface emission and deposition, large-scale advective transport, subscale convective and boundary layer exchanges, chemical and photochemical transformations, as well as wet scavenging. Transport is simulated "off line" from CCM with dynamical variables provided every 3 hours from preestablished history tapes. Advection is calculated using the semi-Lagrangian transport scheme [*Rasch and Williamson,* 1990] developed for the MATCH model of *Rasch et al.* [1997]. Convective and boundary layer transports are expressed according to *Hack* [1994] and *Holtslag and Boville* [1993], respectively. A detailed evaluation of the model results is provided in a companion paper [*Hauglustaine et al.,* this issue]. An analysis of the spatial and temporal variability in the chemical fields predicted by the model suggests that regional events such as summertime ozone episodes in polluted areas can be simulated by MOZART.

1. Introduction

One of the current challenges in atmospheric science is to assess the potential impact of human activities on the chemical composition of the global atmosphere and on the climate system. Energy consumption (mostly fossil fuel) has increased dramatically since the industrial revolution, leading not only to increasing atmospheric abundance of carbon dioxide (CO_2) but also of more reactive species such as methane (CH_4), nonmethane hydrocarbons (NMHCs), carbon monoxide (CO), nitrogen oxides (NO_x), and sulfur dioxide (SO_2). Emissions resulting from changes in land use and specifically from intense agricultural practices and from biomass burning have also contributed to the observed changes in the chemical composition of the atmosphere. The earliest studies devoted to these issues focused mostly on local pollution and regional effects. We now realize that even the most pristine regions of the world are anthropogenically perturbed, so the problem must be addressed at the global scale. Global approaches are necessary to assess the potential impact of human activities on the Earth's climate, on the oxidizing capacity of the atmosphere, and on chemical degradation of the Earth's ecosystems.

Chemical compounds released in the atmosphere are affected by physical and chemical processes. They may be transported over large distances by atmospheric motions, transformed into other compounds by chemical or photochemical processes, and "washed out" or deposited at the Earth's surface. An understanding of the global behavior of chemical compounds requires that these processes be accurately quantified before they can be adequately represented in atmospheric models. This is generally performed either through laboratory experiments or field observations. Models are ideal tools to synthesize existing information within a framework constrained by fundamental laws.

[1]National Center for Atmospheric Research, Boulder, Colorado.
[2]Also at Service d'Aéronomie du Centre National de la Recherche Scientifique, Paris.
[3]Belgian Institute for Space Aeronomy, Brussels.
[4]CIRES, University of Colorado, Boulder, Colorado.
[5]NOAA Aeronomy Laboratory, Boulder, Colorado

Paper number 98JD02397.
0148-0227/98/98JD-02397$09.00

Different attempts have been made to reproduce the global three-dimensional (3-D) distribution of chemical compounds in the stratosphere [e.g., *Grose et al.*, 1987; *Rose and Brasseur*, 1989; *Austin et al.*, 1992; *Granier and Brasseur*, 1992; *Chipperfield et al.*, 1993, 1994, 1995; *Lefèvre et al.*, 1994; *Rasch et al.*, 1995; *Brasseur et al.*, 1997] and in the troposphere [e.g., *Levy et al.*, 1985; *Crutzen and Zimmermann*, 1991; *Penner et al.*, 1991; *Kasibhatla et al.*, 1993; *Kanakidou and Crutzen*, 1993; *Jacob et al.*, 1993; *Müller and Brasseur*, 1995; *Roelofs and Lelieveld*, 1995; *Pham et al.*, 1995; *Kasibhatla et al.*, 1996; *Chin et al.*, 1996; *Kraus et al.*, 1996; *Brasseur et al.*, 1996; *Berntsen and Isaksen*, 1997]. The complexity of the chemistry implemented in these models varies from a few reactions to a relatively detailed formulation. Models with prescribed source/sink terms have been used to establish the global distribution of nearly passive tracers such as CO_2 [*Fung et al.*, 1983], nitrous oxide [*Mahlman and Moxim*, 1978; *Levy et al.*, 1982], halocarbons [*Prather et al.*, 1987], methane [*Fung et al.*, 1991; *Taylor et al.*, 1991] or isotopes such as radon 222 [e.g., *Jacob and Prather*, 1990; *Feichter and Crutzen*, 1990], lead 210 [*Balkanski et al.*, 1993], and krypton 85 [e.g., *Jacob et al.*, 1987].

The purpose of this paper is to present a new chemical transport model called MOZART (model for ozone and related chemical tracers), which is a follow-up of the earlier IMAGES model [*Müller and Brasseur*, 1995]. In this first version of MOZART, which is aimed at studying the global budget of tropospheric ozone and its precursors, the transport is driven by the dynamics of the NCAR Community Climate Model (CCM). In section 2, we provide an overview of MOZART, while the adopted formulation for emissions, atmospheric transport, chemical processes and deposition processes is presented in sections 3, 4, 5, and 6, respectively. The spatial and temporal variability produced by the model is illustrated in section 7. The model results are evaluated through a detailed comparison with observations in a companion paper [*Hauglustaine et al.*, this issue].

2. Model Overview

MOZART (version 1) provides the global distribution of 56 chemical constituents (see Table 1) between the Earth's surface and the pressure level of 3 mbar (approximately 35 km altitude). The concentration of each species is predicted by individually solving a mass conservation equation taking into account advective, convective, and diffusive transport as well as surface and in situ emissions, photochemical conversions, and wet and dry surface deposition. This is accomplished by applying a succession of operators to the volume mixing ratio of species i q_i (t_n) at time step t_n:

$$q_i\,(t_{n+1}) = D \cdot K \cdot C \cdot A \;\; q_i\,(t_n) \qquad (1)$$

where A is the operator for advection, C is the operator for chemistry (including wash-out processes and in situ emissions), K is the operator for convection, and D is the operator for diffusion (including surface emission and dry deposition). The meteorological updates are performed using a progenitor of the MATCH "off line" transport model which is described in detail by *Rasch et al.* [1994, 1997]. Much of the meteorological information is supplied from the NCAR Community Climate model (CCM). The version of CCM used in the present study (CCM-2, Ω 0.5 library) is intermediate between CCM-2 [*Hack et al.*, 1993] and CCM-3 [*Kiehl et al.*, 1996, 1998], with the convective parameterization developed by *Hack* [1994]. The cloud water content and precipitation flux are generated from an early version of the prognostic cloud parameterization recently described by *Rasch and Kristjansson* [1998]. All other meteorological processes are represented according to the parameterizations described by *Kiehl et al.* [1996]. The climate from a very similar version of CCM is briefly described by *Hack and Kiehl* [1995].

MOZART is run at a horizontal resolution of approximately 2.8° in latitude and longitude (64 Gaussian grid cells in latitude and 128 equidistant longitudes), corresponding to a triangular truncation of the spherical harmonic representation at total wavenumber 42 (T42). Figure 1a shows the horizontal grid used in MOZART. In its present configuration the model includes 25 levels in the vertical. The hybrid $\sigma - p$ coordinate, proposed by *Simmons and Strüfing* [1981], is used with spacing between levels stretching slowly through the troposphere and stratosphere from approximately 20 m in the boundary layer to nearly 3.5 km near the rigid lid at the upper boundary of the model, and enhanced vertical resolution in the vicinity of the tropopause (see Figure 1b). The evolution of species due to all physical and chemical processes is calculated with a single numerical time step of 20 min.

Dynamical and other physical variables (see Table 2) needed to calculate the resolved advective transport as well as smaller-scale exchanges and wet scavenging are precalculated by CCM and provided to MOZART every 3 hours from preestablished "history tapes." Within a 3-hour period these variables are interpolated linearly as a function of time. In the case of water vapor the specific humidity calculated by CCM-2 is used only below the tropopause; in the stratosphere the H_2O source associated with methane and molecular hydrogen oxidation is taken into account, and the water vapor mixing ratio $q(H_2O)$ is derived from the hydrogen conservation equation [*Le Texier et al.*, 1988]:

$$q\,(H_2O) = 6 \text{ ppmv} - 2q\,(CH_4) - q\,(H_2) \qquad (2)$$

where the mixing ratio of methane $q(CH_4)$ and of hydrogen $q(H_2)$ are calculated in the chemical transport model.

Climatological variables provided by CCM-2 have been evaluated by *Hack et al.* [1994] and *Hurrell* [1995], and in many cases are consistent with observations; however, some deficiencies were noted and have been

Table 1. Chemical Species Considered in MOZART

Number	Species Name
1	$O_x = O(^3P) + O(^1D) + O_3$
2	$NO_x = N + NO + NO_2$
3	OH
4	HO_2
5	N_2O
6	NO_3
7	HNO_3
8	HO_2NO_2
9	N_2O_5
10	PAN
11	MPAN
12	ONIT
13	CH_4
14	CO
15	H_2
16	C_2H_6
17	C_3H_8
18	C_2H_4
19	C_3H_6
20	C_4H_{10}
21	$C_{10}H_{16}$
22	ISO
23	MVK
24	MACR
25	CH_3COCH_2O
26	CH_3O_2
27	$C_3H_7O_2$
28	$C_2H_5O_2$
29	$C_3H_6OHO_2$
30	$CH_3COCH_2O_2$
31	ISO1
32	MCO_3
33	$MOHO_2$
34	H_2O_2
35	CH_3OOH
36	C_2H_5OOH
37	C_3H_7OOH
38	C_3H_6OHOOH
39	CH_3COCH_2OOH
40	CH_3COOOH
41	CH_2O
42	CH_3CHO
43	CH_2OHCHO
44	CH_3COCHO
45	CH_3CO_3
46	CH_3COCH_3
47	Rn 222
48	Pb 210
49	O_3 stratosphere
50	O_3 inert

PAN, peroxy acetyl nitrate; MPAN, peroxy methacrylic nitrate; C_4H_{10}, surrogate for $\geq C_4$ hydrocarbons; $C_{10}H_{16}$, α-pinene; ISO, isoprene; ISO1, surrogate for peroxy radicals formed from isoprene oxidation; ONIT, surrogate for organic nitrates; MVK, methyl vinyl ketone; MACR, methyl acrolein; $MOHO_2$, peroxy radical formed from MVK oxidation; MCO_3, peroxy methacrylic radical

addressed in a subsequent version of the CCM-2 (library Ω 0.5) described by *Hack and Kiehl* [1995]. This version, which is used to drive MOZART, includes an improved representation of radiative transfer in clear and cloudy atmospheres (with incorporation of radiative effects by CH_4, N_2O, CFC-11, CFC-12, background aerosols, and ice clouds), an updated parameterization of boundary layer dynamics, and land surface exchanges (leading to more realistic estimates of the boundary layer height and of the intensity of the hydrological cycle). As a result, the surface temperature and precipitation rates over continents are more consistent with observations than in earlier versions of CCM.

The distribution of several long-lived species (O_3, NO_x, HNO_3, N_2O_5, CH_4, CO, N_2O) is prescribed above 60 mbar (or approximately 20 km altitude), according to monthly and zonally averaged values, as provided by the middle atmosphere 3-D STARS model [*Brasseur et al.*, 1997].

The architecture of the model is based on a front-end processor that interprets a user input file to form a Fortran 90 source code and input data files for a complete simulation. The model is therefore a flexible tool affording the user control over basic processes such as advection, convection, diffusion, chemistry, and input/output. Spatial grid and time steps and numerical method parameters are completely user specified. With 204,800 grid points in the model domain and for the conditions described in this paper, a 1-year simulation is performed in approximately 200 hours (single CPU) on one of the NCAR C90 CRAY computers (about 60% of the computer time is spent on the chemistry and the remainder for transport of the 50 tracers). About 15 Gb of disk space is needed to store 1 year of input data from the CCM, and 20 Gb of output data are generated by MOZART for a typical 1-year run.

A preliminary version of the model (version 0) was used by *Brasseur et al.* [1996] to investigate the budget of chemical compounds in the Pacific troposphere in conjunction with the Mauna Loa observatory photochemistry experiment (MLOPEX) measurements. Ver-

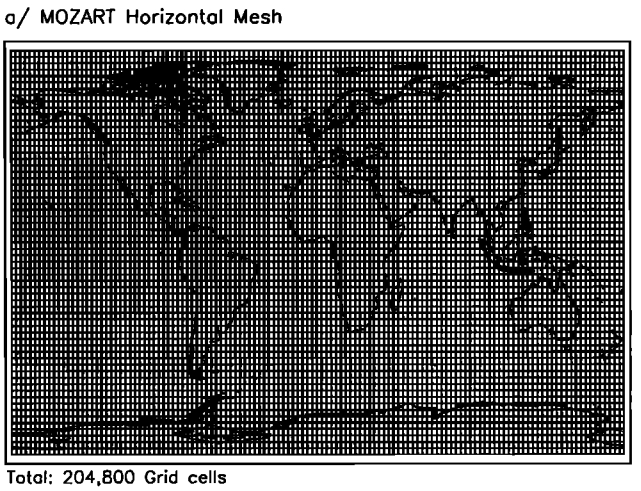

Figure 1. (a) horizontal grid and (b) vertical levels (b) adopted in the MOZART model. Original vertical levels of CCM are represented by solid lines, while added levels are shown by dashed lines.

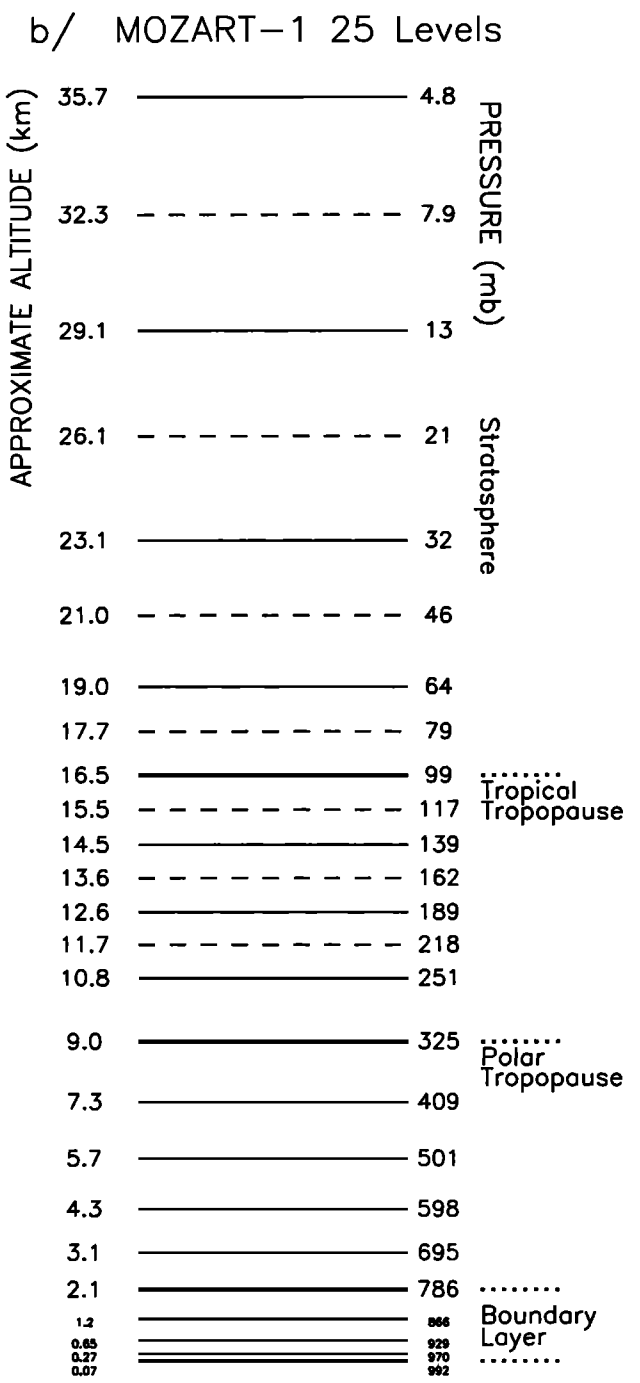

Figure 1. (continued)

sion 0 included a simplified representation of NMHC chemistry with only 22 transported species, 18 levels on the vertical, did not include below-cloud scavenging, and was driven by an earlier version of CCM-2. More recent versions of the model were used by *Hauglustaine et al.* [1998] in a study of ozone over the North Atlantic ocean and by *Emmons et al.* [1997] for a comparison of nitrogen species distributions provided by various chemical transport models (CTMs) and observed climatologies.

3. Emissions

The surface emissions of biogenic and anthropogenic species are based on *Müller* [1992] with some adjustments to account for more recent data. For N_2O, for example, the surface sources from *Nevison* [1994] are adopted, while for nitrogen oxides produced by fossil fuel combustion, the emissions established by *Benkovitz et al.* [1996] are used. Table 3 shows the global emissions for each chemical compound expressed by category. Technological sources include industrial and domestic fossil fuel burning (oil, gas, and coal), waste disposal, and emissions from other industrial activities. Biomass burning accounts for the fires in tropical and nontropical forest, savanna, fuelwood use, and agricultural waste burning. The spatial and temporal distribution of the biomass burned is taken from *Hao and Liu* [1994] in the tropics and from *Müller* [1992] in nontropical regions. The emission ratios of each chemical species relative to CO_2 are taken from *Granier et al.* [1996] for each type of biomass fire except for the CO and NO_x savanna emission where the value suggested by *Hao et al.* [1996] and by *Andreae et al.* [1996] are considered. Biogenic sources over the continent include the emissions of hydrocarbons by vegetation as well as the release of N_2O, NO and CO by soils. In the case of methane the biogenic contribution includes the emissions from ruminants, rice paddies, wetlands, and termites. The model also accounts for the emissions of N_2O, CO, and hydrocarbons by the ocean. For carbon monoxide, the emissions established by *Erickson and Taylor* [1992] for the ocean have been reduced uniformly by a factor of 10 to match the global emission values recently proposed by *Bates et al.* [1995] on the basis of cruise observations.

These global emission distributions are provided as monthly mean values and are linearly interpolated in time for each model time step. Plate 1 shows CO global emissions for January and July. During both seasons, the emissions of CO are large in Europe, the eastern

Table 2. Fields Provided by NCAR CCM2 (Ω0.5) and Used to Drive MOZART

Field	Description	Units
P_s	surface pressure	Pa
D_s	water equivalent snow depth	m
u	zonal wind component	m/s
v	meridional wind component	m/s
T	temperature	K
q	specific humidity	kg/kg
K_c	diffusivity of heat in the boundary layer	m^2/s
γ_c	boundary layer countergradient factor	$1/m^3/m$
f_c	cloud fraction	fraction
W_{H_2O}	water vapor tendency from rainout	kg/kg/s
L	liquid water content	kg/kg
η_c	convective mass flux	$kg/m^2/s$
β_c	convection overshoot parameter	fraction

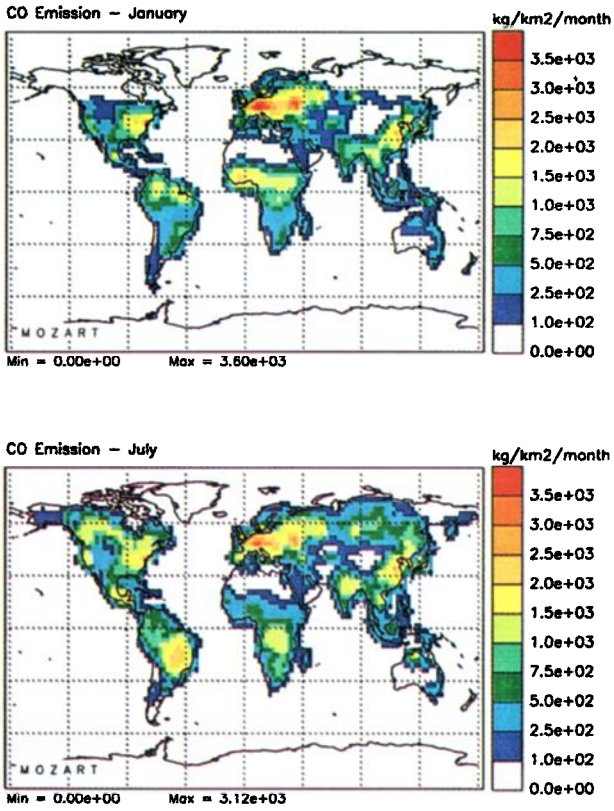

Plate 1. Monthly mean carbon monoxide total surface emission used in MOZART for January and July conditions (kg/km^2/month).

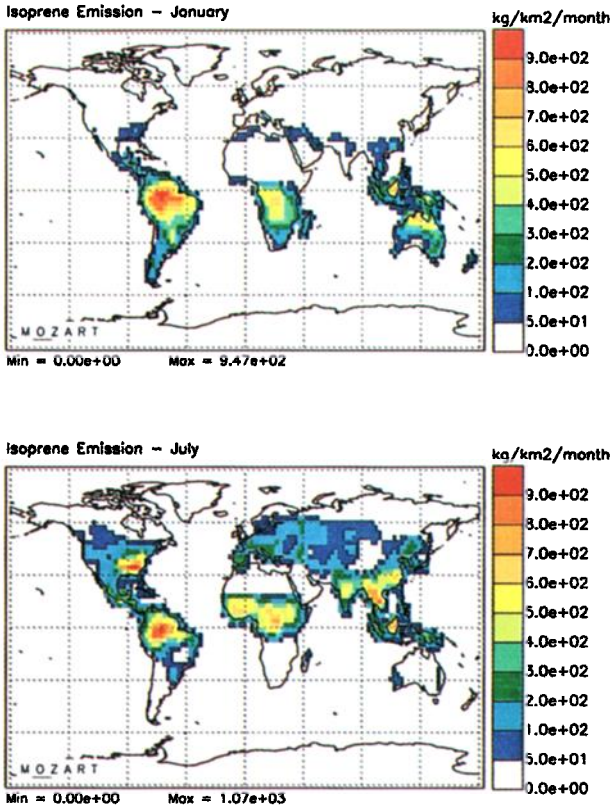

Plate 2. Monthly mean isoprene surface emission used in MOZART for January and July conditions (kg/km^2/month).

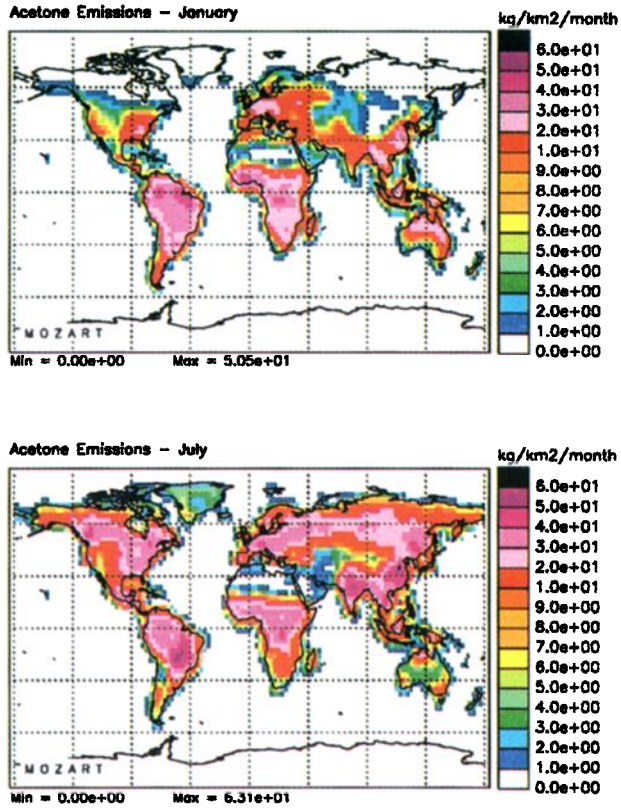

Plate 3. Monthly mean acetone total surface emission used in MOZART for January and July conditions (kg/km^2/month).

United States, and eastern Asia, as a result of fossil fuel combustion, including automobiles. The contribution due to biomass burning is largest in the tropics, and its geographical distribution varies with season. Substantial CO emissions result also from the large fires that occur in the boreal regions at the end of the summer season.

The monthly mean distribution of the isoprene emissions by tree foliage is shown in Plate 2 for January and July. The values are largest in the tropics and, during summertime, over the southeastern United States. The strong seasonal variation in the emission reflects foliage density, and in addition, seasonal changes in temperature and solar insolation. A diurnal cycle is imposed on the isoprene source to account for the empirically known dependences with light intensity and leaf temperature [see *Müller and Brasseur,* 1995]. In the case of terpene emissions (not shown), a day/night ratio is applied to account for the temperature dependence.

Acetone is believed to significantly affect the budget of HO_x (= OH + HO_2) in the upper troposphere [*Jaeglé et al.,* 1997], as well as the formation rate of peroxy acetyl nitrate (PAN) [*Singh et al.,* 1995]. The presence of this carbonyl results from the oxidation of propane and, to a lesser extent, other hydrocarbons, including terpenes. Another source is provided by direct surface emissions associated with vegetation release, biomass burning, and anthropogenic activities. The two latter

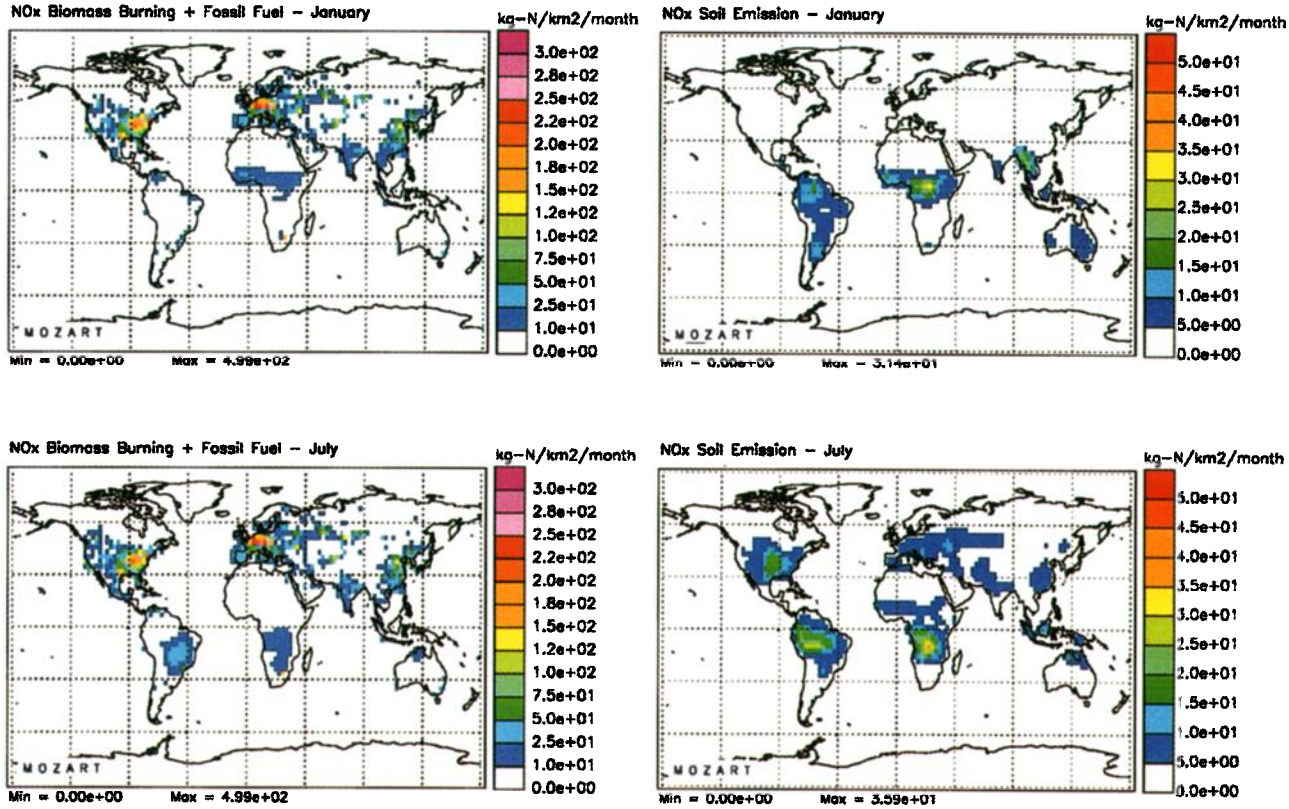

Plate 4. Anthropogenic (left panel) and biogenic (right panel) monthly mean NO_x surface emissions used in MOZART for January and July conditions (kg-N/km^2/month).

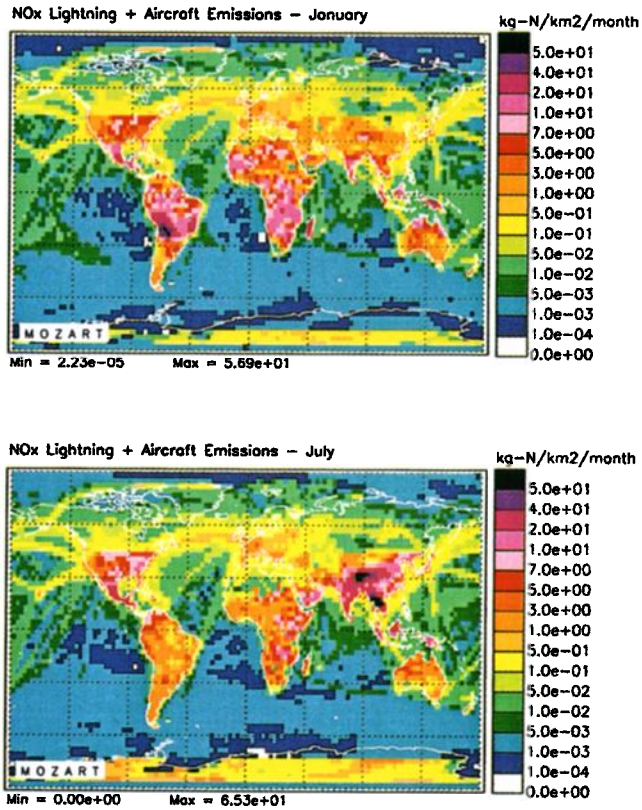

Plate 5. Vertically integrated monthly mean NO_x emission associated with lightning activity and aircraft traffic considered in MOZART for January and July conditions (kg-N/km^2/month).

emissions are distributed geographically as in the case of CO, with a total release of 14 Tg/yr and 1.5 Tg/yr, respectively. The uncertainty on vegetation sources is high, and a provisional working value of 18 Tg/yr is used and distributed according to the net primary productivity (NPP). The resulting surface emission for acetone is shown in Plate 3 (January and July).

The surface emissions of nitrogen oxides (NO_x = NO + NO_2), as used in MOZART, are shown in Plate 4. The largest surface sources are located in industrialized regions and are associated with fossil fuel combustion. Microbial production of NO in soils maximizes in the tropics but is also significant at midlatitudes during summertime. The biomass burning source of NO_x exhibits a maximum over the continents in the tropics.

The atmospheric production of NO_x by lightning and of NO_x, CO, and CH_4 by aircraft traffic is also taken into account. Lightning is assumed to produce 7 TgN/yr of reactive nitrogen which are distributed as a function of space and season according to the location of convective clouds in the CCM and following the parameterization of *Price and Rind* [1992]. In their study, the production of NO_x is assumed to be proportional to $H^{4.9}$ over the continents and $H^{1.73}$ over the ocean, if H represents the height of the top of convective clouds. In MOZART the value where H is determined from the CCM convection and the NO_x production (molecules cm^{-3} s^{-1}) is assumed to be constant with height between the surface and the cloud top. The geographical

Table 3. Global Surface Emissions of Trace Gases Considered in MOZART

Species	Industrial	Agricultural	Biomass Burning	Biogenic	Oceans	Total
CH_4 (Tg/yr)	130.9	179.0	39.4	110.0	9.8	469.1
CO (Tg/yr)	381.6	0.0	661.8	162.1	13.0	1218.5
N_2O (TgN/yr)	1.1	4.3	0.6	5.6	3.8	15.4
NO_x (TgN/yr)	21.4	0.0	7.5	6.6	0	35.5
CH_3COCH_3 (Tg/yr)	1.5	0.0	14.0	18.0	0.0	33.5
CH_2O (Tg/yr)	2.3	0.0	0.0	0.0	0.0	2.3
C_2H_6 (TgC/yr)	6.0	0.0	4.4	0.8	0.8	12.0
C_3H_8 (TgC/yr)	3.8	0.0	2.3	1.6	1.4	9.1
C_2H_4 (TgC/yr)	4.3	0.0	13.6	4.3	8.2	30.4
C_3H_6 (TgC/yr)	1.7	0.0	6.0	0.8	9.9	18.4
C_4H_{10} (TgC/yr)	63.7	0.0	11.3	73.2	58.2	206.4
Isoprene (TgC/yr)	0.0	0.0	0.0	220.0	0.0	220.0
Terpenes (TgC/yr)	0.0	0.0	0.0	129.5	0.0	129.5

distribution of convective clouds and hence of NO_x by lightning evolves with a time step of 3 hours and accounts therefore for some of the diurnal variation in thunderstorm activity. The three-dimensional distribution of the NO_x injection associated with aircraft operation is taken from NASA [*Friedl*, 1997] and corresponds to a total source of about 0.51 Tg-N/yr. Plate 5 shows the distribution of the vertically integrated NO_x produced by lightning and air traffic as adopted in the model in January and July. The lightning source is most intense over the continents, as expected from the observed frequency of lightning strokes, and exhibits a strong seasonal variation. Note that the small NO_x source calculated in the model over Antarctica is likely to be overestimated and results from the convective activity generated by the CCM over this region. Aircraft emissions are visible mostly along transoceanic routes (e.g., North Atlantic and Pacific); their importance is relatively limited over continental regions when thunderstorm activity is strong.

4. Transport Processes

The advective scheme for chemical species used in MOZART is a progenitor of the MATCH transport model developed by *Rasch et al.* [1997]. It uses the shape-preserving semi-Lagrangian formulation proposed by *Williamson and Rasch* [1989] and *Rasch and Williamson* [1990] with Hermite cubic polynomial interpolation. The advection step is subdivided into separate horizontal and vertical substeps. Simulations of quasi-inert species such as chlorofluorocarbons (CFCs) provide an integrated measure of the model performance regarding global transport and, specifically, interhemispheric exchanges. *Hartley et al.* [1994] have evaluated the performance of CCM-2 transport by comparing the concentrations of CFC-11 predicted by the model with observations made at five sites located in different regions of the world [e.g., *Cunnold et al.*, 1994]. This comparison suggests that the semi-lagrangian transport (SLT) scheme driven by CCM-2 winds reproduces many of the key features of atmospheric transport, although some specific aspects of large-scale exchanges (storm track dynamics, cross-equatorial flow) merit further attention. The MATCH "off line" transport model has also been used [*Mahowald et al.*, 1997a] in an inverse mode with assimilated winds to derive surface emissions of CFC-11. The performance of the same transport formulation applied to stratospheric dispersion and cross-tropopause exchanges has been discussed by *Rasch et al.* [1994].

Because semi-Lagrangian transport is inherently non-conservative, a mass conserving correction is applied to the solution after each time step. The original form of the fixer developed for water vapor [*Rasch and Williamson*, 1990] was modified by *Rasch et al.* [1995] for species like ozone with high concentrations in the stratosphere. In the present version of MOZART the mass fixer preserves the sign of the advection tendency (D. Pollard, personal communication, 1997). For each grid cell, the final mixing ratio q_f is calculated from the mixing ratio before advection (q_b) and after advection (q_a) according to

$$q_f = q_b + \alpha\,(q_a - q_b) \tag{3}$$

where α is a constant chosen to ensure global conservation [*Rasch et al.*, 1995] and defined by

$$\alpha = \begin{cases} 0.5\frac{\Delta M^+ + \Delta M^-}{\Delta M^+} & q_a > q_b \\ 0.5\frac{\Delta M^+ + \Delta M^-}{\Delta M^-} & q_a < q_b \end{cases} \tag{4}$$

with ΔM^+ and ΔM^- defined, respectively, as

$$\Delta M^+ = \int_v \max\,(q_a\rho_a - q_b\rho_b, 0)\,dV \tag{5a}$$

$$\Delta M^- = \int_v \max\,(q_b\rho_b - q_a\rho_a, 0)\,dV \tag{5b}$$

if V is the volume of the entire atmospheric domain. Following this procedure, for grid cells where the SLT tends to increase (decrease) the mixing ratio, the increase (decrease) is reduced by a factor α.

Intrusion of stratospheric air substantially affects the tropospheric distribution of chemical species like ozone and nitrogen oxides, whose mixing ratio increases rapidly with height above the tropopause [*Levy et al.*, 1985; *Tie and Hess*, 1997]. Because cross-tropopause exchanges often occur through folds associated with jet stream disturbances and cutoff lows, an accurate representation of these subgrid processes is not straightforward in global chemical transport models. Model simulations have shown that in the case of chemical species with strong vertical gradients in the vicinity of the tropopause (*e.g.*, O_3, NO_x), the mass correction provided by the "fixer" was undesirably large and that the error was probably maximum near the tropopause. To partially address this issue, the vertical resolution used in CCM (18 levels) has been increased to 25 levels, with a vertical space increment of approximately 1 km near the tropopause (see Figure 1b). The dynamical fields provided by CCM (at its original resolution) are vertically interpolated on the MOZART grid. With this modification of the model, mass conservation is improved, and the calculated vertical profiles of ozone in the upper troposphere are closer to the observations. The replacement of the semi-Lagrangian formulation currently used in MOZART by a new Eulerian scheme (flux form) is expected to further address this problem in the model [*Rasch and Lawrence*, 1998]. Another cause for inaccuracies in the calculated concentrations is the errors associated with the winds provided by CCM near the tropopause. A future version of MOZART will use assimilated wind fields, which should be more representative of the actual dynamics in the upper troposphere and lower stratosphere.

Conservative convective transport of chemical tracers is parameterized by the mass flux scheme developed by *Hack* [1994]. This scheme, which represents all types of moist convection in the version 2 of the CCM, adjusts the moist static energy over three adjacent layers (allowing for entrainment in the bottom layer and detrainment in the upper layer). This parameterization has been evaluated [see also *Mahowald et al.*, 1995, 1997b] by comparing calculated distributions of radon 222 (lifetime of 5.5 days) with observed values. Because of the very limited data set available [*Liu et al.*, 1984], no definitive conclusion can be drawn from this comparison. As suggested by Figure 2, however, the vertical distributions of this radionuclide seem to be well reproduced by MOZART over the North American continent during wintertime. In the summer, however, when convective activity is more intense, vertical transport over the continents seems too weak in the model; as a consequence, ^{222}Rn concentrations are overestimated in the boundary layer and underestimated in the upper troposphere. The comparison between the calculated and the observed seasonal variations of ^{222}Rn, shown in Figure 3, seems to indicate that large-scale and synoptic scale transport of the isotope are well represented in MOZART, except at Mauna Loa and Dumont d'Urville, where the model values are smaller than suggested by the observations. The discrepancy at Mauna Loa was previously reported by *Mahowald* [1996] and *Jacob et al.* [1997] and tentatively attributed to an anomalously high ^{222}Rn source in eastern Asia.

Boundary layer exchanges are derived according to *Holtslag and Boville* [1993] by expressing the vertical eddy flux $\overline{w'c'}$ (molecules cm^{-2} s^{-1}) by

$$\overline{w'c'} = -K_c \left[\frac{dc}{dz} - \gamma_c \right] \tag{6}$$

where c (molecules cm^{-3}) is the species density, and K_c is an eddy diffusion coefficient (cm^2 s^{-1}) which depends on a turbulent velocity scale and on the Richardson number dependent boundary layer height. Variable γ_c is a countergradient term representing non local transport associated with dry boundary layer convection. The resulting prognostic equation for boundary layer transport (which also accounts for surface emission and dry deposition) is solved using the implicit scheme of *Richtmyer and Morton* [1967].

5. Chemistry

The chemical scheme used in MOZART and given in Tables 4 and 5 is very similar to the scheme implemented previously in the IMAGES model [*Müller and Brasseur*, 1995]. It includes 107 gas phase and 5 heterogeneous reactions and 28 photochemical reactions. These reactions emphasize the processes affecting tropospheric ozone and its precursors. Rate constants for most chemical reactions are taken from *DeMore et al.* [1997]. For some reactions involving organic compounds, values are provided by other sources (as stated in Table 4). The effects of nonmethane hydrocarbons are represented by the degradation mechanisms of ethane (C_2H_6), propane (C_3H_8), ethylene (C_2H_4), propylene (C_3H_6), isoprene (C_5H_8), terpenes (as α-pinene, $C_{10}H_{16}$), and a lumped compound (C_4H_{10} or n-butane), which is intended to be a surrogate for the other hydrocarbons ($\geq C_4$, excluding isoprene and terpenes). Heterogeneous reactions of N_2O_5 and NO_3 on sulfate aerosols (which are believed to provide an important loss mechanism for NO_x during nighttime) are parameterized using the empirical first-order reaction rate used in IMAGES (see *Müller and Brasseur* [1995] for more details). The spatial distribution of sulfate aerosols ($SO_4^=$) is taken from the model of *Pham et al.* [1995]. Little information is available for heterogeneous reactions involving other species, especially organic compounds; we have assumed for methylvinylketone (MVK) and methylacrolein (MACR) a loss rate identical to that used for N_2O_5 and NO_3. Future devel-

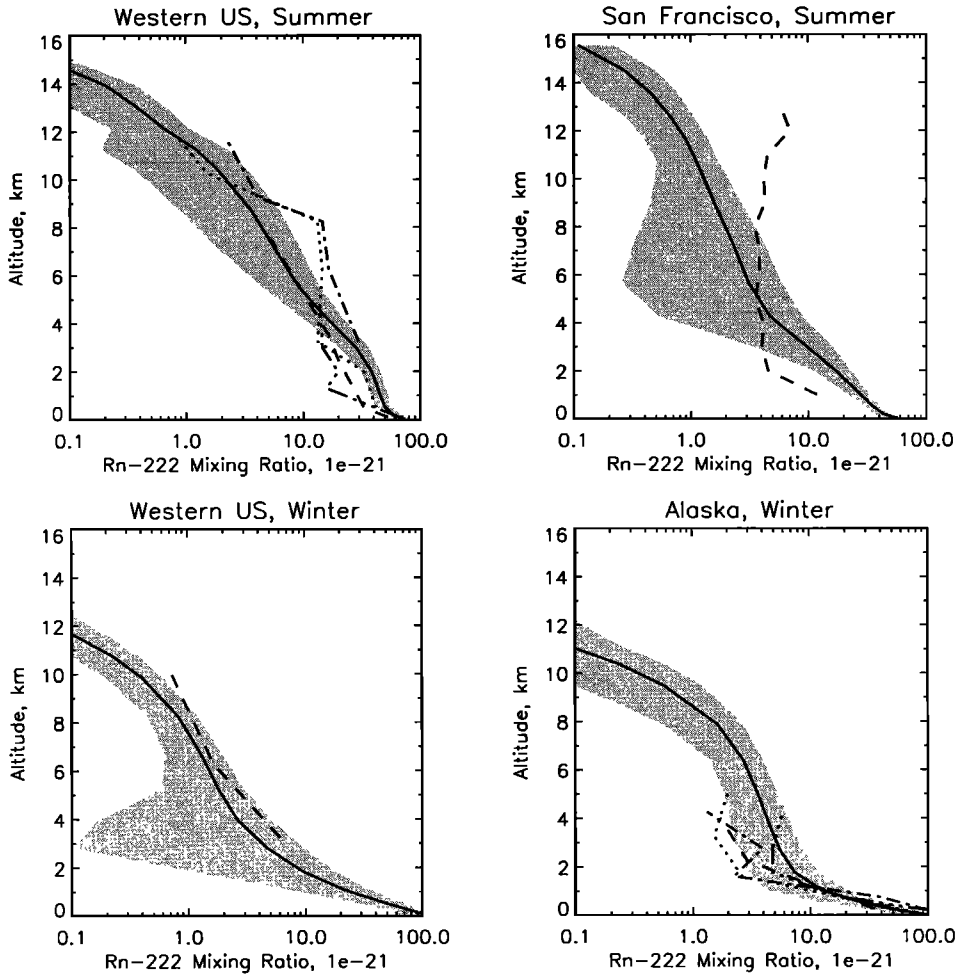

Figure 2. Observed (dashed lines) and calculated (solid line is monthly average, and shaded area is the 1-σ standard deviation) ^{222}Rn vertical profiles (10^{-21}) over selected regions during summer (top) and winter (bottom). Measurements are taken from *Liu et al.* [1984] except over San Francisco [M. Kritz, personal communication, 1997].

opments of the model will consider the chemical role played by other types of particles (e.g., ammonium aerosols [*Dentener and Crutzen*, 1994], mineral dust [*Dentener et al.*, 1996], and carbonaceous aerosols [*Lary et al.*, 1997; *Hauglustaine et al.*, 1996]). In the present stage of its development, MOZART does not account for chemical reactions in the aqueous phase. A scheme addressing some of these processes is currently under development.

The photolysis frequencies (j) are derived from pretabulated values through a multivariate log linear interpolation through a Taylor series expansion [*Burden and Faires*, 1985]. The discrete-ordinate radiative model used to establish this table is the troposphere ultraviolet visible (TUV) code of S. Madronich (personal communication, 1998) which includes 137 spectral intervals and 51 vertical levels. Clear-sky photodissociation coefficients are tabulated for 18 pressure levels, 7 values of the ozone column (as calculated by MOZART), 8 solar zenith angles, and 4 values of the surface albedo. To account for the temperature dependence of the absorption cross sections, the j values are calculated for 6 temperature profiles determined by 3 temperature values specified at 500 mb and 2 temperature values specified at 200 mb. References for absorption cross sections and quantum yields are given in Table 5. The effect of cloudiness on the photolysis frequencies is parameterized according to *Chang et al.* [1987]:

$$j_{\mathrm{cld}}(p) = j_{\mathrm{clr}}(p)\left[1 + F_{\mathrm{above}}(p) + F_{\mathrm{in}}(p) + F_{\mathrm{below}}(p)\right] \tag{7}$$

where $j_{\mathrm{cld}}(p)$ is the cloud-corrected photolysis rate at pressure level p, j_{clr} is the clear-sky rate, and F_{above}, F_{in}, and F_{below} are the correction factors applied above, within or below the clouds, respectively.

Below the clouds,

$$F_{\mathrm{below}}(p) = \left(1.6\cos\chi\; t_r\left(p, p_{\mathrm{top}}\right) - 1\right) f_c\left(p, p_{\mathrm{top}}\right) \tag{8a}$$

where χ is the local zenith angle, $t_r\left(p, p_{\mathrm{top}}\right)$ is the total transmissivity of light from pressure level p_{top} at the top of the model domain to level p, and $f_c\left(p, p_{\mathrm{top}}\right)$ is the vertically averaged cloud cover from level p to p_{top}.

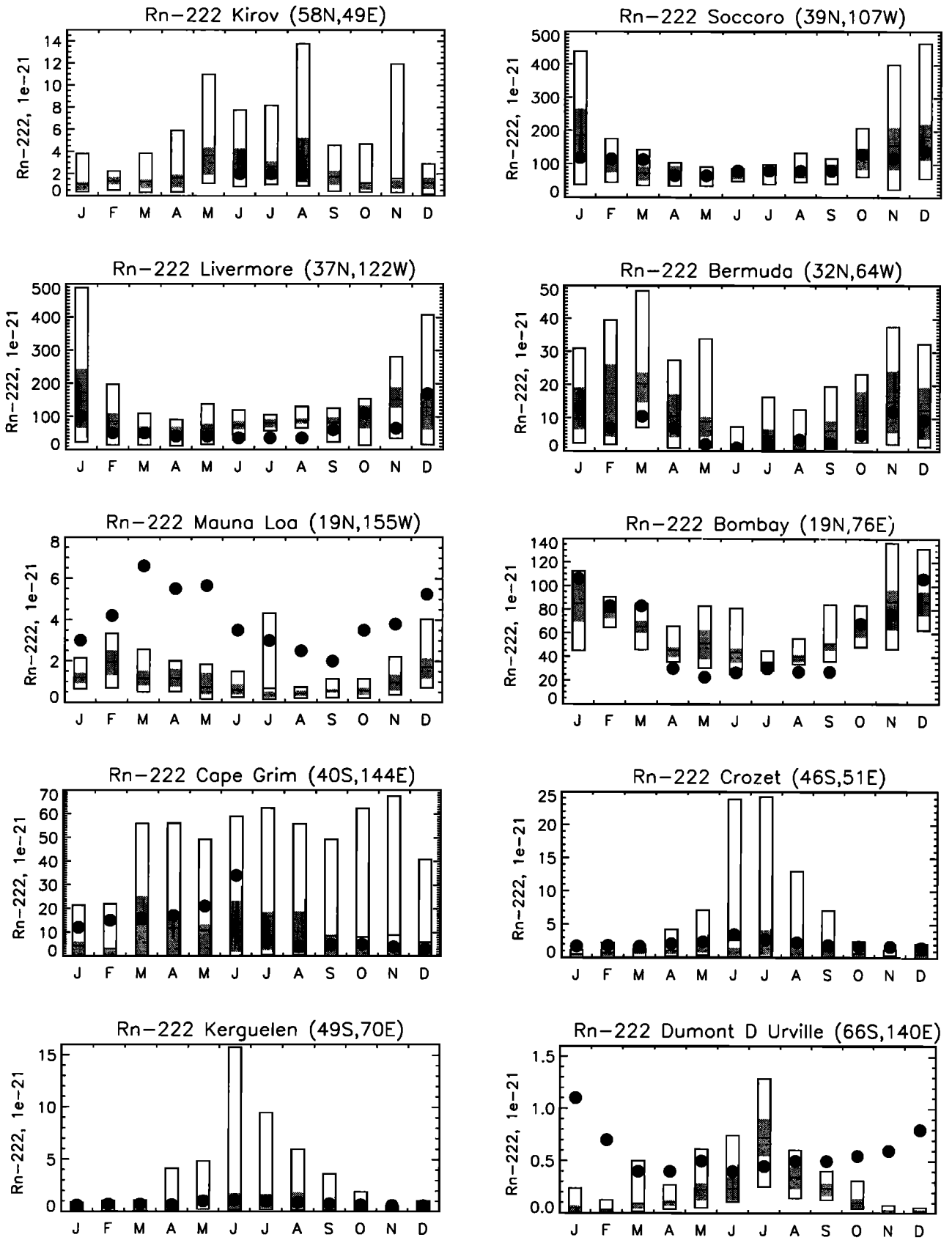

Figure 3. Observed (circles) and calculated (boxes) seasonal cycle of ^{222}Rn mixing ratio (10^{-21}) at selected stations. The model results show the monthly mean (solid line), the median (dashed line), the inner 50th percentile (shaded area), and the range (box).

Table 4. Chemical Reactions Considered in MOZART

	Reaction	Rate	Refs
(R1)	$O(^1D) + N_2 \rightarrow O + N_2$	$k_1 = 1.80E\text{-}11\ \exp(110/T)$	1
(R2)	$O(^1D) + O_2 \rightarrow O + O_2$	$k_2 = 3.20E\text{-}11\ \exp(70/T)$	1
(R3)	$O(^1D) + H_2O \rightarrow 2\ OH$	$k_3 = 2.20E\text{-}10$	1
(R4)	$O + O_2 + M \rightarrow O_3 + M$	$k_4 = 6.00E\text{-}34\ [M]\ (300/T)^{2.3}$	1
(R5)	$O + O_3 \rightarrow 2\ O_2$	$k_5 = 8.00E\text{-}12\ \exp(-2060/T)$	1
(R6)	$O + OH \rightarrow HO_2 + O_2$	$k_6 = 2.20E\text{-}11\ \exp(120/T)$	1
(R7)	$O + HO_2 \rightarrow OH + O_2$	$k_7 = 3.00E\text{-}11\ \exp(200/T)$	1
(R8)	$OH + O_3 \rightarrow HO_2 + O_2$	$k_8 = 1.60E\text{-}12\ \exp(-940/T)$	1
(R9)	$HO_2 + O_3 \rightarrow OH + 2\ O_2$	$k_9 = 1.10E\text{-}14\ \exp(-500/T)$	1
(R10)	$HO_2 + HO_2 \rightarrow H_2O_2$	$k_{10} = (k_a + k_b)\ k_c$ $k_a = 2.30E\text{-}13\ \exp(600/T)$ $k_b = 1.70E\text{-}33\ [M]\ \exp(1000/T)$ $k_c = 1 + 1.40E\text{-}21\ [H_2O]\ \exp(2200/T)$	1
(R11)	$H_2O_2 + OH \rightarrow H_2O + HO_2$	$k_{11} = 2.90E\text{-}12\ \exp(-160/T)$	1
(R12)	$OH + HO_2 \rightarrow H_2O + O_2$	$k_{12} = 4.80E\text{-}11\ \exp(250/T)$	1
(R13)	$OH + OH \rightarrow H_2O + O$	$k_{13} = 4.20E\text{-}12\ \exp(-240/T)$	1
(R14)	$H_2 + OH \rightarrow H_2O + HO_2$	$k_{14} = 5.50E\text{-}12\ \exp(-2000/T)$	1
(R15)	$H_2 + O(^1D) \rightarrow HO_2 + OH$	$k_{15} = 1.00E\text{-}10$	1
(R16)	$N_2O + O(^1D) \rightarrow 2\ NO$	$k_{16} = 6.70E\text{-}11$	1
(R17)	$N_2O + O(^1D) \rightarrow N_2 + O_2$	$k_{17} = 4.90E\text{-}11$	1
(R18)	$N + O_2 \rightarrow NO + O$	$k_{18} = 1.50E\text{-}11\ \exp(-3600/T)$	1
(R19)	$N + NO \rightarrow N_2 + O$	$k_{19} = 2.10E\text{-}11\ \exp(100/T)$	1
(R20)	$NO + HO_2 \rightarrow NO_2 + OH$	$k_{20} = 3.50E\text{-}12\ \exp(250/T)$	1
(R21)	$NO + O_3 \rightarrow NO_2 + O_2$	$k_{21} = 2.00E\text{-}12\ \exp(-1400/T)$	1
(R22)	$NO_2 + O \rightarrow NO + O_2$	$k_{22} = 6.50E\text{-}12\ \exp(120/T)$	1
(R23)	$NO_2 + O_3 \rightarrow NO_3 + O_2$	$k_{23} = 1.20E\text{-}13\ \exp(-2450/T)$	1
(R24)	$NO_3 + HO_2 \rightarrow 0.4\ HNO_3 + 0.6\ OH + 0.6\ NO_2$	$k_{24} = 2.30E\text{-}12\ \exp(170/T)$	2
(R25)	$NO_2 + NO_3 + M \rightarrow N_2O_5 + M$	$k_0 = 2.20E\text{-}30\ (300/T)^{3.9}$ $k_\infty = 1.50E\text{-}12\ (300/T)^{0.7}$ $F_c = 0.6$	1
(R26)	$N_2O_5 + M \rightarrow NO_2 + NO_3 + M$	$k_{26} = k_{25}\ 3.7E26\ \exp(-11000/T)$	1
(R27)	$N_2O_5 + H_2O \rightarrow 2\ HNO_3$	$k_{27} = 2.00E\text{-}21$	1
(R28)	$NO_2 + OH + M \rightarrow HNO_3 + M$	$k_0 = 2.50E\text{-}30\ (300/T)^{4.4}$ $k_\infty = 1.60E\text{-}11\ (300/T)^{1.7}$ $F_c = 0.6$	1
(R29)	$HNO_3 + OH \rightarrow NO_3 + H_2O$	$k_{29} = k_a + 7.20E\text{-}15\ \exp(785/T)$ $k_a = k_b\ /\ (1 + k_b\ /\ k_c)$ $k_b = 1.90E\text{-}33\ \exp(725/T)\ [M]$ $k_c = 4.10E\text{-}16\ \exp(1440/T)$	1
(R30)	$NO_3 + NO \rightarrow 2\ NO_2$	$k_{30} = 1.50E\text{-}11\ \exp(170/T)$	1
(R31)	$NO_2 + HO_2 + M \rightarrow HO_2NO_2 + M$	$k_0 = 1.80E\text{-}31\ (300/T)^{3.2}$ $k_\infty = 4.70E\text{-}12\ (300/T)^{1.4}$ $F_c = 0.6$	1
(R32)	$HO_2NO_2 + M \rightarrow HO_2 + NO_2 + M$	$k_{32} = k_{31}\ 4.7E26\ \exp(-10900/T)$	1
(R33)	$HO_2NO_2 + OH \rightarrow H_2O + NO_2 + O_2$	$k_{33} = 1.30E\text{-}12\ \exp(380/T)$	1
(R34)	$CH_4 + OH \rightarrow CH_3O_2 + H_2O$	$k_{34} = 2.45E\text{-}12\ \exp(-1775/T)$	1
(R35)	$CH_4 + O(^1D) \rightarrow CH_3O_2 + OH$	$k_{35} = 1.40E\text{-}10$	1
(R36)	$CH_4 + O(^1D) \rightarrow H_2 + CH_2O$	$k_{36} = 1.40E\text{-}11$	1
(R37)	$CH_3O_2 + NO \rightarrow CH_2O + NO_2 + HO_2$	$k_{37} = 3.00E\text{-}12\ \exp(280/T)$	1
(R38)	$CH_3O_2 + CH_3O_2 \rightarrow 1.4\ CH_2O + 0.8\ HO_2$	$k_{38} = 2.50E\text{-}13\ \exp(190/T)$	1
(R39)	$CH_3O_2 + HO_2 \rightarrow CH_3OOH + O_2$	$k_{39} = 3.80E\text{-}13\ \exp(800/T)$	1
(R40)	$CH_3OOH + OH \rightarrow 0.58\ CH_3O_2 + 0.42\ OH + 0.42\ CH_2O$	$k_{40} = 3.80E\text{-}12\ \exp(200/T)$	1
(R41)	$CH_2O + OH \rightarrow CO + H_2O + HO_2$	$k_{41} = 1.10E\text{-}11$	1
(R42)	$CH_2O + NO_3 \rightarrow CO + HO_2 + HNO_3$	$k_{42} = 6.00E\text{-}13\ \exp(-2058/T)$	3
(R43)	$CO + OH \rightarrow CO_2 + HO_2$	$k_{43} = 1.50E\text{-}13\ (1 + 0.6\ P)$	1
(R44)	$C_2H_6 + OH \rightarrow C_2H_5O_2 + H_2O$	$k_{44} = 8.70E\text{-}12\ \exp(-1070/T)$	1
(R45)	$C_2H_5O_2 + NO \rightarrow CH_3CHO + HO_2 + NO_2$	$k_{45} = 2.60E\text{-}12\ \exp(365/T)$	1
(R46)	$C_2H_5O_2 + HO_2 \rightarrow C_2H_5OOH + O_2$	$k_{46} = 7.50E\text{-}13\ \exp(700/T)$	1
(R47)	$C_2H_5O_2 + CH_3O_2 \rightarrow 0.7\ CH_2O + 0.8\ CH_3CHO + HO_2$	$k_{47} = 3.75E\text{-}13\ \exp(-40/T)$	4
(R48)	$C_2H_5O_2 + C_2H_5O_2 \rightarrow 1.6\ CH_3CHO + 1.2\ HO_2$	$k_{48} = 6.50E\text{-}14$	1
(R49)	$C_2H_5OOH + OH \rightarrow 0.5\ C_2H_5O_2 + 0.5\ CH_3CHO + 0.5\ OH$	$k_{49} = 3.80E\text{-}12\ \exp(200/T)$	4
(R50)	$C_3H_8 + OH \rightarrow C_3H_7O_2 + H_2O$	$k_{50} = 1.00E\text{-}11\ \exp(-660/T)$	1

Table 4. (continued)

	Reaction	Rate	Refs
(R51)	$C_3H_7O_2 + NO \rightarrow 0.82\ CH_3COCH_3 + NO_2 + HO_2$	$k_{51} = 4.20E\text{-}12\ \exp(180/T)$	5
(R52)	$C_3H_7O_2 + HO_2 \rightarrow C_3H_7OOH + O_2$	$k_{52} = 7.50E\text{-}13\ \exp(700/T)$	6
(R53)	$C_3H_7O_2 + CH_3O_2 \rightarrow 0.5\ CH_2O + HO_2 + 0.82\ CH_3COCH_3$	$k_{53} = 3.75E\text{-}13\ \exp(-40/T)$	6
(R54)	$C_3H_7OOH + OH \rightarrow H_2O + C_3H_7O_2$	$k_{54} = 3.80E\text{-}12\ \exp(200/T)$	6
(R55)	$CH_3COCH_3 + OH \rightarrow CH_3COCH_2O_2 + H_2O$	$k_{55} = 2.20E\text{-}12\ \exp(-685/T)$	1
(R56)	$CH_3COCH_2O_2 + NO \rightarrow CH_3COCH_2O + NO_2$	$k_{56} = 4.20E\text{-}12\ \exp(180/T)$	6
(R57)	$CH_3COCH_2O_2 + HO_2 \rightarrow CH_3COCH_2OOH + O_2$	$k_{57} = 7.50E\text{-}13\ \exp(700/T)$	6
(R58)	$CH_3COCH_2OOH + OH \rightarrow CH_3COCH_2O_2 + H_2O$	$k_{58} = 3.80E\text{-}12\ \exp(200/T)$	6
(R59)	$CH_3COCH_2O + M \rightarrow CH_3CO_3 + CH_2O + M$	$k_{59} = 8.70E{+}13\ \exp(-7300/T)$	6
(R60)	$CH_3COCH_2O + O_2 \rightarrow CH_3COCHO + HO_2$	$k_{60} = 6.50E\text{-}14\ \exp(-1400/T)$	6
(R61)	$C_4H_{10} + OH \rightarrow 0.8\ ISO1$	$k_{61} = 1.55E\text{-}11\ \exp(-540/T)$	7
(R62)	$C_3H_6 + OH + M \rightarrow C_3H_6OHO_2 + M$	$k_0 = 8.00E\text{-}27\ (300/T)^{3.5}$ $k_\infty = 3.00E\text{-}11$ $F_c = 0.5$	5
(R63)	$C_3H_6 + O_3 \rightarrow 0.532\ CH_2O + 0.585\ HO_2 + 0.4275\ OH + 0.08\ CH_4 + 0.37\ CO + 0.5\ CH_3CHO + 0.2875\ CH_3O_2$	$k_{63} = 6.50E\text{-}15\ \exp(-1900/T)$	1
(R64)	$C_3H_6 + NO_3 \rightarrow ONIT$	$k_{64} = 4.00E\text{-}15$	4
(R65)	$C_3H_6OHO_2 + NO \rightarrow CH_3CHO + CH_2O + HO_2 + NO_2$	$k_{65} = 4.20E\text{-}12\ \exp(180/T)$	4
(R66)	$C_3H_6OHO_2 + HO_2 \rightarrow C_3H_6OHOOH + O_2$	$k_{66} = 6.50E\text{-}13\ \exp(650/T)$	4
(R67)	$C_3H_6OHOOH + OH \rightarrow 0.5\ C_3H_6OHO_2 + 0.5\ OH + H_2O$	$k_{67} = 3.80E\text{-}12\ \exp(200/T)$	4
(R68)	$CH_3CHO + OH \rightarrow CH_3CO_3 + H_2O$	$k_{68} = 5.60E\text{-}12\ \exp(270/T)$	1
(R69)	$CH_3CHO + NO_3 \rightarrow CH_3CO_3 + HNO_3$	$k_{69} = 1.40E\text{-}12\ \exp(-1900/T)$	1
(R70)	$CH_3CO_3 + NO \rightarrow CH_3O_2 + CO_2 + NO_2$	$k_{70} = 5.30E\text{-}12\ \exp(360/T)$	1
(R71)	$CH_3CO_3 + NO_2 + M \rightarrow PAN + M$	$k_0 = 9.70E\text{-}29\ (300/T)^{5.6}$ $k_\infty = 9.30E\text{-}12\ (300/T)^{1.5}$ $F_c = 0.6$	1
(R72)	$PAN + M \rightarrow CH_3CO_3 + NO_2 + M$	$k_{72} = k_{71}\ 1.11E28\ \exp(-14000/T)$	1
(R73)	$CH_3CO_3 + HO_2 \rightarrow 0.67\ CH_3COOOH + 0.33\ CH_3COOH + 0.33\ O_3$	$k_{73} = 4.30E\text{-}13\ \exp(1040/T)$	1
(R74)	$CH_3CO_3 + CH_3O_2 \rightarrow CH_3O_2 + CH_2O + HO_2 + CO_2$	$k_{74} = 1.80E\text{-}09\ \exp(-1800/T)$	8
(R75)	$CH_3CO_3 + CH_3O_2 \rightarrow CH_2O + CH_3COOH + O_2$	$k_{75} = 4.10E\text{-}15\ \exp(2100/T)$	8
(R76)	$CH_3CO_3 + CH_3CO_3 \rightarrow 2\ CH_3O_2 + 2\ CO_2$	$k_{76} = 2.90E\text{-}12\ \exp(500/T)$	1
(R77)	$CH_3COOOH + OH \rightarrow CH_3CO_3 + H_2O$	$k_{77} = 1.00E\text{-}11$	4
(R78)	$C_2H_4 + OH + M \rightarrow 0.6667\ C_3H_6OHO_2 + M$	$k_0 = 1.00E\text{-}28\ (300/T)^{0.8}$ $k_\infty = 8.80E\text{-}12$ $F_c = 0.6$	1
(R79)	$C_2H_4 + O_3 \rightarrow CH_2O + 0.52\ HO_2 + 0.42\ CO$	$k_{79} = 1.20E\text{-}14\ \exp(-2630/T)$	1
(R80)	$ISO + OH \rightarrow ISO1$	$k_{80} = 2.50E\text{-}11\ \exp(450/T)$	4
(R81)	$ISO + O_3 \rightarrow 0.66\ MACR + 0.26\ MVK + 0.45\ O + 0.7825\ CH_2O + 0.06\ HO_2 + 0.68\ OH + 0.07\ C_3H_6 + 0.19\ CO$	$k_{81} = 1.20E\text{-}14\ \exp(-2013/T)$	9
(R82)	$ISO + NO_3 \rightarrow ONIT$	$k_{82} = 3.03E\text{-}12\ \exp(-446/T)$	9
(R83)	$ISO1 + NO \rightarrow 0.42\ MVK + 0.58\ MACR + CH_2O + HO_2 + NO_2$	$k_{83} = 3.70E\text{-}12\ \exp(180/T)$	4
(R84)	$ISO1 + NO \rightarrow 0.59\ CH_3CO_3 + CH_2O + 0.59\ CH_2OHCHO + 0.59\ NO_2 + 0.41\ ONIT$	$k_{84} = 5.00E\text{-}13\ \exp(180/T)$	4
(R85)	$ISO1 + HO_2 \rightarrow 0.126\ MVK + 0.174\ MACR + 0.3\ CH_2O + 0.3\ HO_2$	$k_{85} = 7.50E\text{-}13\ \exp(750/T)$	9
(R86)	$ISO1 + CH_3O_2 \rightarrow MACR + 2\ CH_2O + 2\ HO_2$	$k_{86} = 1.30E\text{-}14$	4
(R87)	$ISO1 + CH_3CO_3 \rightarrow MACR + HO_2 + CH_2O$	$k_{87} = 4.90E\text{-}14$	4
(R88)	$MVK + OH \rightarrow MOHO_2$	$k_{88} = 4.13E\text{-}12\ \exp(452/T)$	9
(R89)	$MVK + O_3 \rightarrow 0.05\ CO + 0.06\ HO_2 + 0.04\ CH_3CHO + 0.82\ CH_3COCHO + 0.8\ CH_2O + + 0.2\ O + .08\ OH$	$k_{89} = 4.00E\text{-}15\ \exp(-2000/T)$	9
(R90)	$MACR + OH \rightarrow 0.5\ MOHO_2 + 0.5\ MCO_3$	$k_{90} = 1.86E\text{-}11\ \exp(175/T)$	9
(R91)	$MACR + O_3 \rightarrow 0.275\ HO_2 + 0.215\ OH + 0.8\ CH_3COCHO + 0.7\ CH_2O + 0.2\ O + 0.2\ CO$	$k_{91} = 4.40E\text{-}15\ \exp(-2500/T)$	9
(R92)	$MOHO_2 + NO \rightarrow CH_2OHCHO + CH_3CO_3 + NO_2$	$k_{92} = 3.50E\text{-}12\ \exp(180/T)$	4
(R93)	$MOHO_2 + NO \rightarrow ONIT$	$k_{93} = 4.50E\text{-}13\ \exp(180/T)$	4
(R94)	$MOHO_2 + HO_2 \rightarrow 0.3\ CH_3CO_3 + 0.3\ CH_2OHCHO$	$k_{94} = 7.50E\text{-}13\ \exp(700/T)$	4
(R95)	$CH_2OHCHO + OH \rightarrow 0.5\ CH_3CO_3 + 0.5\ HO_2$	$k_{95} = 6.00E\text{-}12\ \exp(250/T)$	4
(R96)	$CH_2OHCHO + NO_3 \rightarrow CH_3CO_3 + HNO_3$	$k_{96} = 1.40E\text{-}12\ \exp(-1900/T)$	4
(R97)	$MCO_3 + NO \rightarrow CH_3COCH_2O + NO_2$	$k_{97} = 2.40E\text{-}11$	1
(R98)	$MCO_3 + NO_2 \rightarrow MPAN$	$k_0 = 9.70E\text{-}29\ (300/T)^{5.6}$ $k_\infty = 9.30E\text{-}12\ (300/T)^{1.5}$ $F_c = 0.6$	1
(R99)	$MPAN + M \rightarrow MCO_3 + NO_2 + M$	$k_{99} = k_{86}\ 1.11E28\ \exp(-14000/T)$	1

Table 4. (continued)

	Reaction	Rate	Refs
(R100)	$MCO_3 + HO_2 \rightarrow MOHO_2$	k_{100}= 4.50E-13 exp(1040/T)	4
(R101)	$MCO_3 + CH_3O_2 \rightarrow CH_2O + HO_2 + CH_3COCH_2O$	k_{101} = 2.20E-12 exp(490/T)	8
(R102)	$MCO_3 + CH_3CO_3 \rightarrow CH_3COCH_2O + CH_3O_2$	k_{102} = 5.00E-12 exp(550/T)	4
(R103)	$MCO_3 + MCO_3 \rightarrow 2\ CH_3COCH_2O$	k_{103} = 2.50E-12 exp(550/T)	4
(R104)	$ONIT + OH \rightarrow NO_2 + MOHO_2$	k_{104} = 6.80E-13	4
(R105)	$C_{10}H_{16} + OH \rightarrow 1.64\ ISO1 + CH_3COCH_3$	k_{105} = 1.20E-11 exp(444/T)	10
(R106)	$C_{10}H_{16} + O_3 \rightarrow 1.122\ MACR + 0.442\ MVK + 0.765\ O + 1.156\ OH + 0.119\ C_3H_6 + 1.326\ CH_2O + 0.323\ CO + 0.102\ HO_2$	k_{106} = 9.90E-16 exp(-730/T)	4
(R107)	$C_{10}H_{16} + NO_3 \rightarrow 1.7\ ISO1 + NO_2$	k_{107} = 5.60E-11 exp(-650/T)	4
(R108)	$N_2O_5 + SO_4^{=} \rightarrow HNO_3 + HNO_3$	k_{108} = f([$SO_4^{=}$], T, [H_2O])	4
(R109)	$NO_3 + SO_4^{=} \rightarrow HNO_3$	k_{109} = f([$SO_4^{=}$], T, [H_2O])	4
(R110)	$MVK + SO_4^{=} \rightarrow$ Products	k_{110} = f([$SO_4^{=}$], T, [H_2O])	4
(R111)	$MACR + SO_4^{=} \rightarrow$ Products	k_{111} = f([$SO_4^{=}$], T, [H_2O])	4
(R112)	$CH_3COCHO + SO_4^{=} \rightarrow$ Products	k_{112} = f([$SO_4^{=}$], T, [H_2O])	4

Read 1.80E-11 as 1.80×10^{-11}. T is temperature (K), [M] atmospheric density (cm^{-3}), [H_2O] water vapor density (cm^{-3}), P pressure (hPa), [$SO_4^{=}$] sulfate density. References: 1, *DeMore et al.* [1997]; 2, *Hall et al.* [1988]; 3, *Cantrell et al.* [1985]; 4, *Müller and Brasseur* [1995]; 5, *Atkinson et al.* [1996]; 6, *Kanakidou et al.* [1991]; 7, *Atkinson* [1985]; 8, *Moorgat et al.* [1989]; 9, *Zimmermann and Poppe* [1996]; 10, *Carter* [1990]. The three-body reaction rates are calculated from

$$k = \frac{k_0[\mathrm{M}]}{1 + k_0[\mathrm{M}]/k_\infty} F_c^{\left\{1+[\lg(k_0[\mathrm{M}]/k_\infty)]^2\right\}^{-1}}$$

Table 5. Photolytic Reactions Considered in MOZART

	Reaction	Refs
(R1)	$O_2 + h\nu \rightarrow O + O$	1
(R2)	$O_3 + h\nu \rightarrow O(^1D) + O_2$	1
(R3)	$O_3 + h\nu \rightarrow O + O_2$	1
(R4)	$N_2O + h\nu \rightarrow O(^1D) + N_2$	1
(R5)	$NO + h\nu \rightarrow N + O$	1
(R6)	$NO_2 + h\nu \rightarrow NO + O$	1
(R7)	$N_2O_5 + h\nu \rightarrow NO_2 + NO_3$	1
(R8)	$HNO_3 + h\nu \rightarrow NO_2 + OH$	1
(R9)	$NO_3 + h\nu \rightarrow 0.89\ NO_2 + 0.11\ NO + 0.89\ O_3$	2
(R10)	$HO_2NO_2 + h\nu \rightarrow NO_2 + HO_2$	1
(R11)	$CH_3OOH + h\nu \rightarrow CH_2O + HO_2 + OH$	1
(R12)	$CH_2O + h\nu \rightarrow CO + 2\ HO_2$	1
(R13)	$CH_2O + h\nu \rightarrow CO + H_2$	1
(R14)	$H_2O + h\nu \rightarrow OH + HO_2$	1
(R15)	$H_2O_2 + h\nu \rightarrow OH + OH$	1
(R16)	$CH_3CHO + h\nu \rightarrow CH_3O_2 + CO + HO_2$	2
(R17)	$C_3H_6OHOOH + h\nu \rightarrow CH_3CHO + CH_2O + HO_2 + OH$	3
(R18)	$CH_3COOOH + h\nu \rightarrow CH_3O_2 + OH$	3
(R19)	$PAN + h\nu \rightarrow CH_3CO_3 + NO_2$	1
(R20)	$MPAN + h\nu \rightarrow MCO_3 + NO_2$	3
(R21)	$CH_2OHCHO + h\nu \rightarrow CH_2O + CO + 2\ HO_2$	3
(R22)	$MACR + h\nu \rightarrow MCO_3 + CO + 0.6\ CH_3COCHO + 0.4\ CH_3CO_3 + 0.4\ CH_2O + 2.6\ HO_2$	3
(R23)	$MVK + h\nu \rightarrow CH_3CO_3 + HO_2 + 0.25\ CH_2O + 0.25\ CO$	3
(R24)	$C_2H_5OOH + h\nu \rightarrow CH_3CHO + HO_2 + OH$	3
(R25)	$C_3H_7OOH + h\nu \rightarrow 0.82\ CH_3COCH_3 + OH + HO_2$	4
(R26)	$CH_3COCH_2OOH + h\nu \rightarrow CH_3COCH_2O + OH$	4
(R27)	$CH_3COCH_3 + h\nu \rightarrow CH_3CO_3 + CH_3O_2$	5
(R28)	$CH_3COCHO + h\nu \rightarrow CH_3CO_3 + CO + HO_2$	2

References: 1, *DeMore et al.* [1997]; 2, *Madronich and Calvert* [1989]; 3, *Müller and Brasseur* [1995]; 4, *Kanakidou et al.* [1991]; 5, *Gierczak et al.* [1998].

Within the cloud,

$$F_{\text{in}}(p) = (1.4\cos\chi - 1) \cdot f_c(p) \qquad (8b)$$

and above the clouds,

$$F_{\text{above}}(p) = \alpha_i \left(1 - t_r\left(p_s, p\right)\right) \cdot \cos\chi f_c\left(p_s, p\right) \qquad (8c)$$

where $t_r(p_s, p)$ is the total transmissivity between the surface and the level p, and $f_c(p_s, p)$ is the vertically averaged cloud fraction between p_s and p. Value α_i is a reaction dependent coefficient given by *Chang et al.* [1987, Table 2]. Expressions (8a), (8b), and (8c) are used only for local zenith angles χ less than 60°. For $\chi \geq 60°$, the values of the correction factors are evaluated at $\chi = 60°$ [*Chang et al.*, 1987].

The transmissivity between levels p_1 and p_2 is calculated according to

$$t_r\left(p_1, p_2\right) = \frac{5 - e^{\tau(p_1, p_2)}}{4 + 0.42\,\tau\left(p_1, p_2\right)} \qquad (9)$$

where $\tau(p_1, p_2)$ is the cloud optical depth between levels p_1 and p_2 [*Chang et al.*, 1987]. The cloud extinction optical depth is expressed as a function of the liquid water content L (g water/g air) and the cloud fraction f_c [*Slingo*, 1989; *Hack et al.*, 1993]:

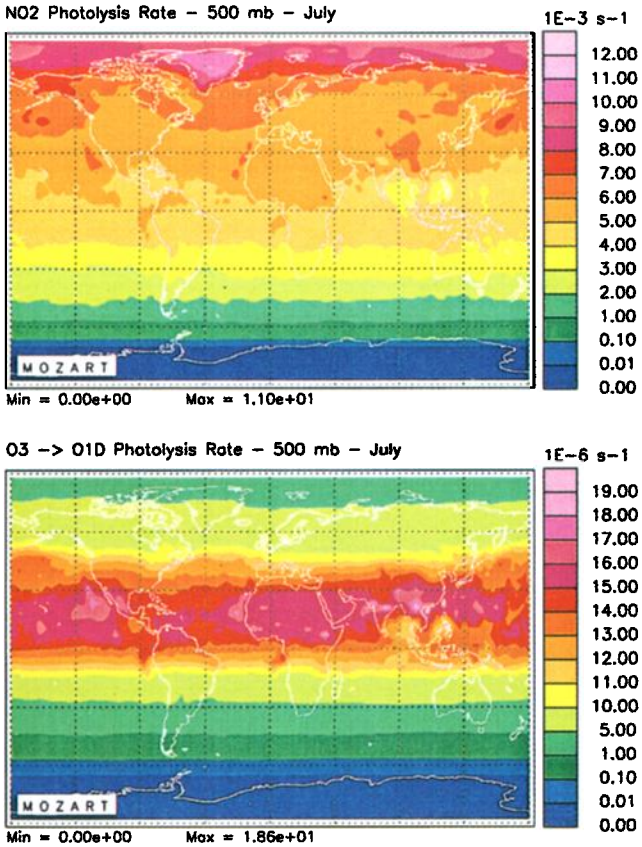

Plate 6. Distribution of NO_2 and O_3 to $O(^1D)$ photolysis rates calculated in MOZART for July conditions at 500 mbar (10^{-3}/s).

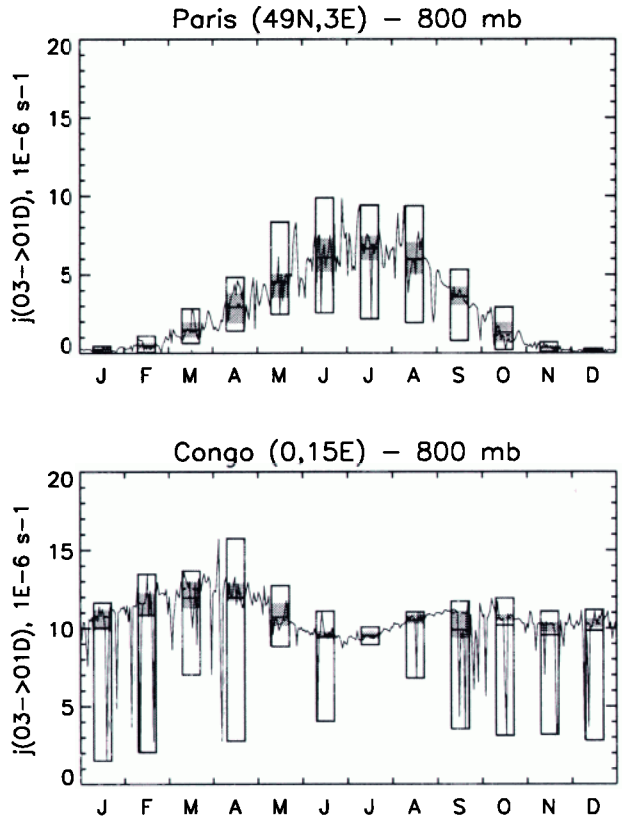

Figure 4. Seasonal variation of ozone to $O(^1D)$ photolysis rates (10^{-6}/s) calculated by MOZART at 800 mbar at midlatitudes (49°N, 3°E) and in the tropics (0°N, 15°E). The solid line represents the day-to-day variability, and the box plot shows the monthly mean (solid line), the median (dashed line), the 50th percentile (shaded area), and the range (box).

$$\tau\left(p_1, p_2\right) = \frac{\left(A + B/r_e\right)}{g} \int_{p_1}^{p_2} L(p) \cdot f_c^{1.5}(p) dp \qquad (10)$$

where r_e is the effective cloud droplet radius (10 μm), $A = 280$ cm^2 g^{-1}, $B = 13{,}000$ μm cm^2 g^{-1}, and where g = 981 cm s^{-2} is the gravitational acceleration. The distributions of L and f_c are provided every 3 hours by CCM as three-dimensional fields (see Table 2).

For illustration, Plate 6 shows the quasi-horizontal distribution of the 24-hour average NO_2 and of O_3 photolysis frequencies (channel leading to $O(^1D)$ formation) at 500 mbar for July conditions. The photolysis frequency of NO_2 is highest at high latitudes during summertime where the daily integrated solar flux (in the spectral region of 350-400 nm with weak atmospheric absorption) is largest because the length of the day reaches 24 hours. In the case of the ozone photodissociation, a substantial fraction of the photolytic light (near 300 nm) is absorbed by stratospheric ozone, and hence the diurnal averaged j value is highest in the tropics, where the ozone column is low. The longitudinal variations seen in the photolysis coefficients are associated with the distribution of surface albedo and cloudiness. Figure 4 details the temporal variability of

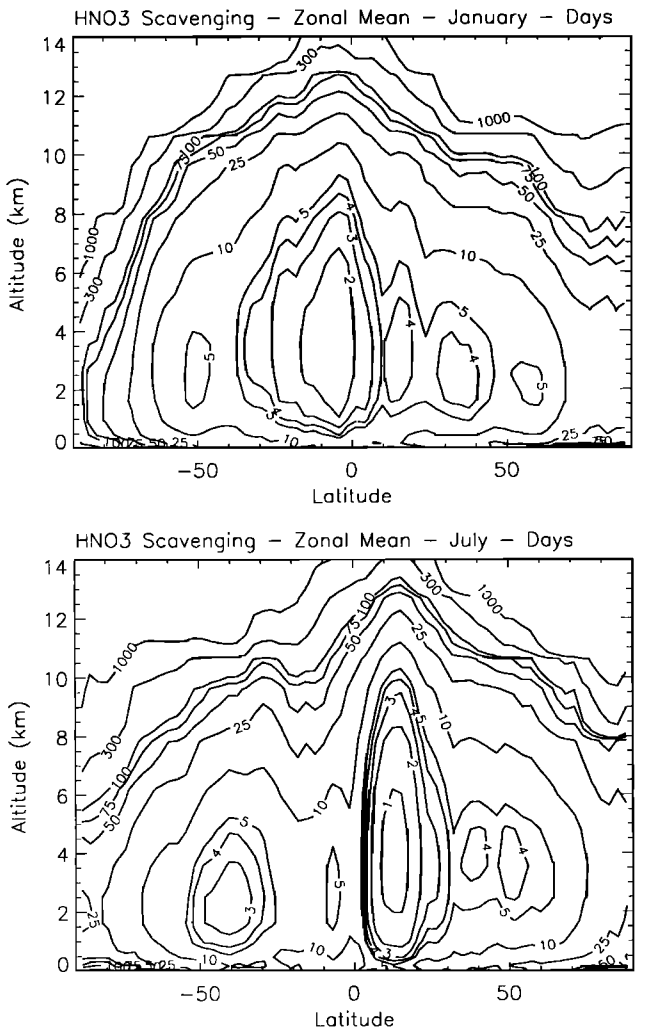

Figure 5. Zonally averaged HNO_3 lifetime (days) associated with wet removal processes calculated for January and July conditions.

the ozone j value ($\lambda < 310$ nm) as produced by the model at a pressure level of 800 mbar for midlatitudes (Paris, France) and equatorial (Brazzaville, Congo) conditions. The difference between the two cases is evident: at Paris, a strong summer maximum is visible, while at Brazzaville, the j value remains nearly constant during the year with, however, a weak semiannual signal (maximum values at the equinoxes). The day-to-day variability is associated with the passage of clouds. Depleted photolysis coefficients result from the presence of clouds above the level of 800 mbar, while enhanced photodissociation is produced when clouds are present below that level.

Within the MOZART system, a simulation may vary from a single inert tracer to a complex set of chemically coupled species. MOZART allows species to be grouped into chemical families, thereby reducing the computational burden. In the present configuration of the model, only two chemical families are formed: O_x (=O_3 + $O(^3P)$ + $O(^1D)$), and NO_x (=N + NO + NO_2). The other species are treated individually. The numerical methods adopted in MOZART to solve the chemical system result from a compromise between computational efficiency and accuracy. Chemical compounds may be partitioned into any of five numerical algorithms: explicit Euler forward, linearized Euler backward iterated (EBI) with the Gauss Seidel scheme, quasi-steady-state approximation (QSSA) [*Hesstvedt et al.*, 1978], fully implicit Euler backward with Newton-Raphson iteration, and implicit Runge-Kutta (specifically the RODAS solver described by *Sandu et al.* [1996]). In the present study, three long-lived species, N_2O, CH_4, and CO, are solved via the explicit method, while for other species, the EBI method with five iterations is used.

6. Deposition Processes

Wet deposition is represented as a first-order loss process

$$\left(\frac{dc_g}{dt}\right)_w = -\beta c_g$$

where c_g (molecules cm^{-3}) is the gas phase number density, β (s^{-1}) is the so-called loss coefficient, and t (s) is time. Presently, in-cloud scavenging is formulated for all soluble species (CH_3OOH, C_3H_7OOH, C_3H_6OHOOH, CH_3COCH_2OOH, CH_3COOOH, C_2H_5OOH, HO_2NO_2, ONIT, CH_2O), except nitric acid and hydrogen peroxide, by the parameterization of *Giorgi and Chameides* [1985]. The corresponding loss coefficient for the soluble species (in clouds) is expressed by

$$\beta = \frac{W_{H_2O}}{X_{H_2O} + A/(HRT)} \tag{11}$$

where W_{H_2O} is the rainwater tendency (g cm^{-3} s^{-1}) associated with convective and non convective precipitation (provided by the CCM), X_{H_2O} (g cm^{-3}) is the mass density of convective and non convective raindrops, A is the Avogadro number, R is the perfect gas constant (8.205 10^{-2} atm cm^3 K^{-1} M^{-1} g^{-1}), T is the temperature (Kelvin), and H is the effective Henry's law constant (M atm^{-1}).

In the case of the most soluble species (HNO_3 and H_2O_2), which are also removed efficiently through below-cloud scavenging by rain droplets [*Levine and Schwartz*, 1982], the first-order loss coefficient is derived from the following relation:

$$\beta = -\frac{1}{c_g}\frac{dc_g}{dt} = \frac{1}{c_g}\frac{dc_a}{dt} \tag{12}$$

if c_a (molecules cm^{-3}) is the concentration of the dissolved molecule inside the drop at altitude z (or at pressure p). Expressing again the raindrop density by X_{H_2O}, the surface area density of raindrops by S and their volume density by V, the concentration of the dissolved molecules along the falling path of the drops (expressed as a number of molecules per volume of air) can

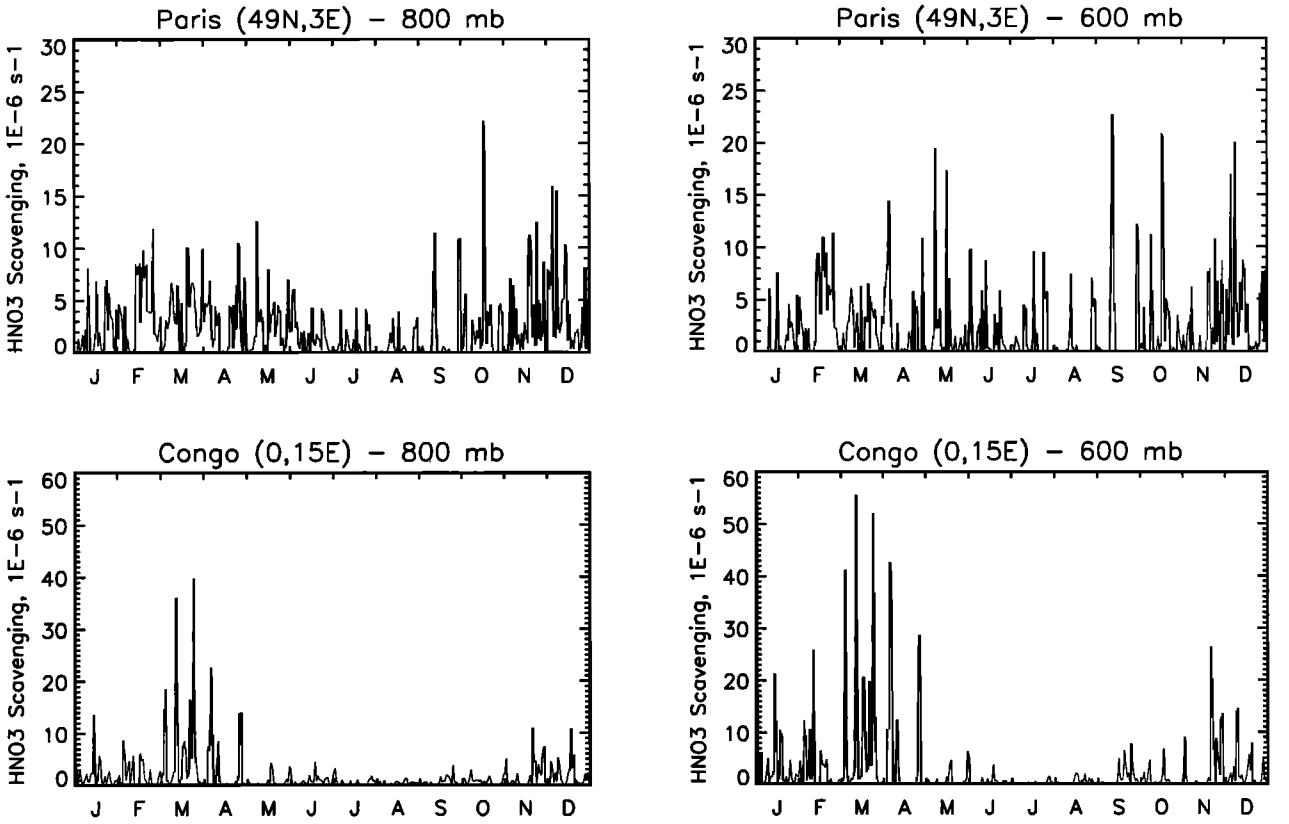

Figure 6. Seasonal cycle of HNO_3 wet removal first-order loss rate (10^{-6}/s) calculated at 800 mbar and 600 mbar at midlatitudes (49°N, 3°E) and in the tropics (0°N, 15°E).

be evaluated from the continuity equation

$$\frac{dc_a}{dt} = F\frac{S}{Vm_{H_2O}}X_{H_2O} = \frac{6FX_{H_2O}}{m_{H_2O}d} \qquad (13)$$

since $S/V = 6/d$, and where d is the effective drop diameter (estimated according to the method of *Best* [1950ab] and *Roelofs and Lelieveld* [1995]) and m_{H_2O} = 1 g (water)/cm^3 (water) is the liquid water density. The rate F (cm^{-2} s^{-1}) of uptake of a gas molecule by a drop can be expressed as

$$F = K_g\left(c_g - c_g^*\right) \qquad (14)$$

where c_g (molecules cm^{-3}) is the concentration of the molecule in the gas phase (air), c_g^* (molecules cm^{-3}) is the concentration of the molecule at the surface of the drop (assumed to be much smaller than c_g [*Fenton et al.*, 1980]), and where the mass-transfer coefficient K_g (cm s^{-1}) is estimated by the semiempirical expression [*Frossling*, 1938]:

$$K_g = \frac{D_g}{d}\left[2 + 0.6\left(\frac{dw_D}{v}\right)^{\frac{1}{2}}\left(\frac{v}{D_g}\right)^{\frac{1}{3}}\right] \qquad (15)$$

wherein v is the kinematic viscosity of air (0.0618 cm^2 s^{-1}), D_g the diffusive coefficient (0.112 cm^2/s), and w_D is the drop terminal velocity (whose value is fixed to 800 cm/s according to *Best* [1950a] and *Beard* [1976]) for equivalent raindrop diameters of about 3 mm. Thus the first-order coefficient β describing the loss of HNO_3 and H_2O_2 by rainwater inside and below the clouds can be expressed as

$$\beta = \frac{6K_g\left(w_D\right)X_{H_2O}}{m_{H_2O}d} \qquad (16)$$

Note that this scheme ignores evaporation of raindrops along their falling path.

Figure 5 shows an example of the lifetime associated with scavenging (expressed in days^{-1}) calculated for nitric acid for January and July conditions (zonal mean). As expected, wash-out is most efficient in the intertropical convergence zone with a typical characteristic time of 0.5-2 days. A secondary maximum associated with the passage of fronts is found at midlatitudes with a corresponding time constant of 3-5 days. In the upper troposphere (14 km in the tropics, 8 km at midlatitudes, 5 km at high latitudes), a typical time constant against wet deposition is 2-3 weeks. It should be noted, however, that wash-out rates are extremely variable in space and time, as shown, for example, in Figure 6, which represents the evolution of the calculated scavenging rate β during July in midlatitudes (Paris) and in the tropics (Congo). In Paris the successive rainfall episodes associated with frontal activity are visible dur-

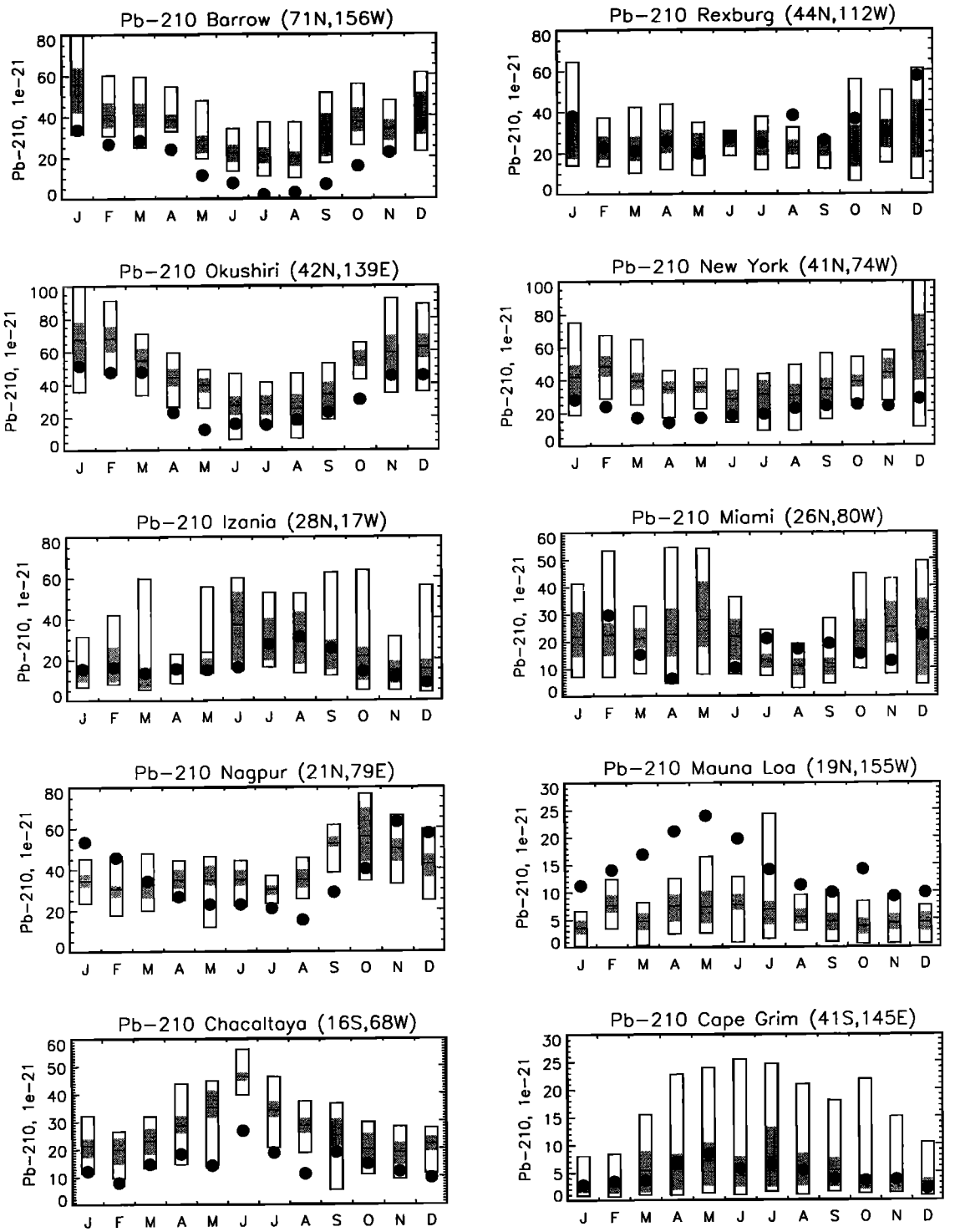

Figure 7. Observed (circles) and calculated (boxes) seasonal cycle of ^{210}Pb mixing ratio (10^{-21}) at selected stations. The model results show the monthly mean (solid line), the median (dashed line), the inner 50th percentile (shaded area) and the range (box).

Table 6. Dry Deposition Velocities Used in MOZART (cm/s)

Species	Land[a]	Ocean	Sea Ice
O_3	0.33, 0.40, 0.46, 0.67	0.075	0.075
NO_x	0.20, 0.24, 0.28, 0.40	0.055	0.055
HNO_3	2.0	1.0	0.055
PAN, MPAN	0.11, 0.13, 0.15, 0.22	0.025	0.025
Organic nitrates	1.1, 1.2, 1.3, 1.5	1.0	0.05
H_2O_2	1.1, 1.2, 1.3, 1.5	1.0	0.05
Organic peroxides	0.55, 0.60, 0.65, 0.75	0.5	0.025
CH_2O	0.33, 0.40, 0.46, 0.67	0.075	0.075
CH_3COCHO	1.1, 1.2, 1.3, 1.5	1.0	0.05
CO	0.01–0.1[b]	0.0	0.0
CH_3COCH_3	0.01–0.1[b]	0.0	0.0
CH_4	10^{-6}–10^{-4}[b]	0.0	0.0
Pb 210	0.2	0.05	0.05

[a]Over bare ground and grass, savanna, nontropical forests, and tropical forests.
[b]Based on *Müller and Brasseur* [1995]; only a typical range is provided here.

ing all seasons, while in the Congo, the existence of a wet season (December-April) and a dry season (May-October) is reproduced by the model.

The performance of the model regarding wash-out can be tested by comparing calculated and observed concentrations of lead 210 (which is produced by radioactive decay of radon 222 and aggregates on aerosols before being efficiently removed from the atmosphere by wet scavenging). For this purpose, we assume, as did other authors [*Balkanski et al.*, 1993; *Lee and Feichter*, 1995; *Rehfeld and Heinmann*, 1995], that the first-order scavenging coefficient is identical for nitric acid and for lead. Figure 7 shows that the seasonal variation of the lead mixing ratio is generally well represented by MOZART, although the concentrations are somewhat overestimated by the model at several conti-

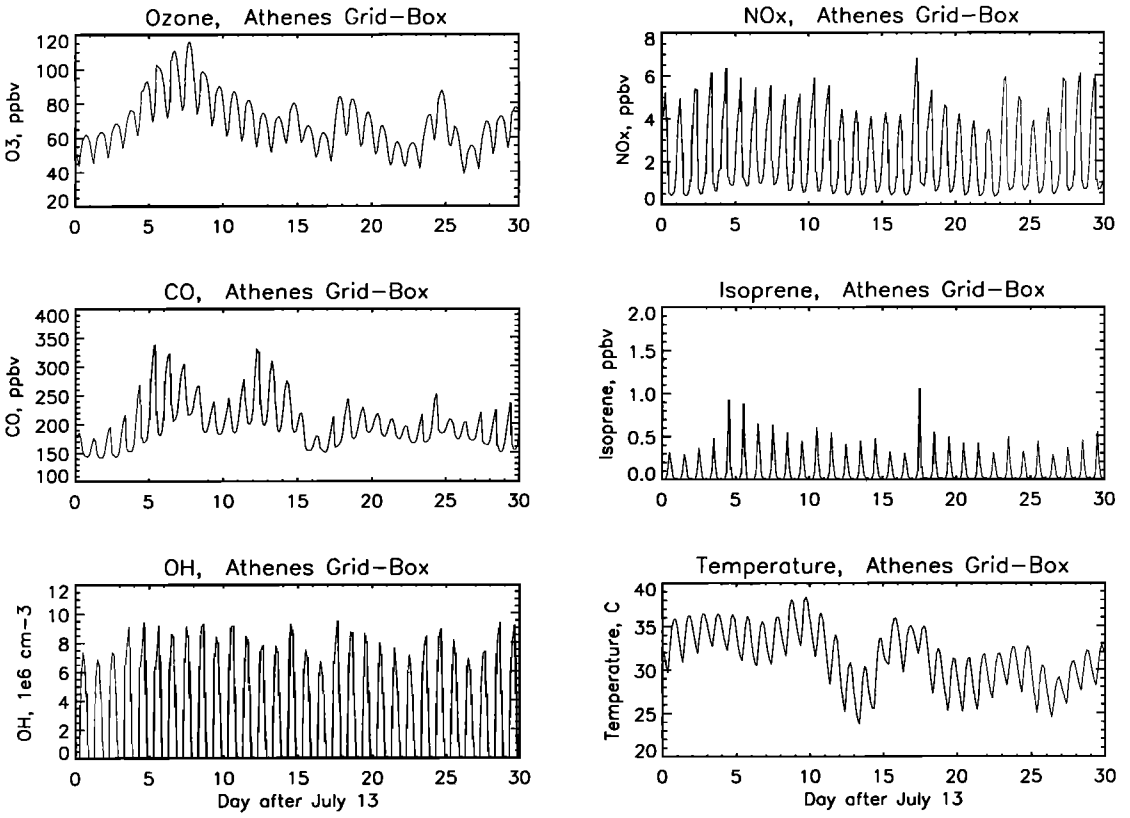

Figure 8. Day-to-day variability of O_3, NO_x, CO, and isoprene mixing ratio (ppbv), OH density (10^6/cm^3), and temperature (°C) calculated for the Athens (Greece) grid cell during July 13 and August 13.

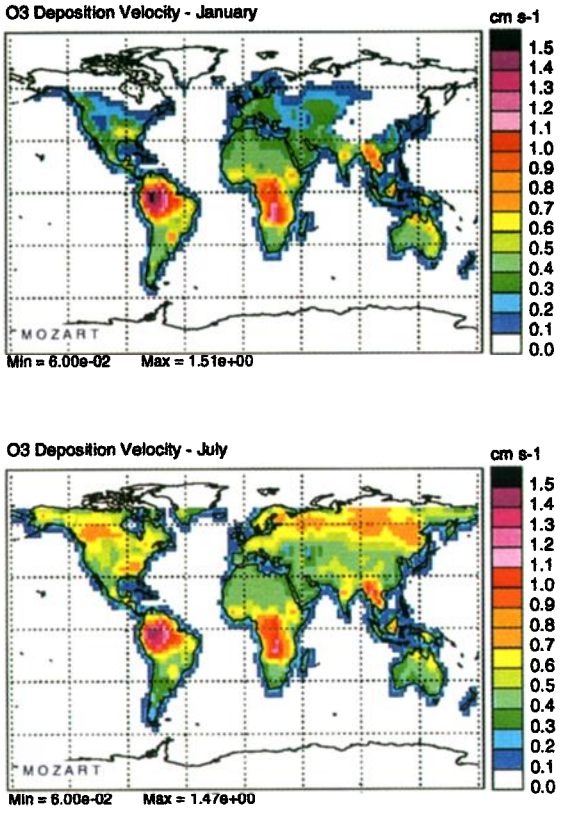

Plate 7. Monthly mean O_3 surface dry deposition velocity (cm/s) considered in MOZART for January and July conditions.

nental stations of North America, South America, and Japan. Discrepancies could be attributed to inaccuracies in the emission and the atmospheric transport of radon, in the intensity of precipitation used for the calculation (in this case, we use the precipitation rates provided by CCM), or in the scavenging scheme. The underestimate of the lead abundance at Mauna Loa, especially during springtime, is probably associated with the underestimate of the ^{222}Rn concentration at the same station. The overestimate by the model of lead 210 at Barrow is due to an underprediction of rainfall by the CCM at high latitudes. Note, however, that the seasonal variation of the lead 210 abundance at this station is well reproduced by the model.

Dry deposition velocities ($v_d = 1/(r_a + r_s)$) are expressed as a function of a specified species independent aerodynamic resistance r_a of 50 s/m and a species dependent surface resistance r_s [*Müller*, 1992]. This later resistance depends on surface types (tropical and nontropical forests, savanna, bare ground, water, ice, and snow) and varies empirically with temperature [*Müller*, 1992]. The ratio between daytime and nighttime deposition velocities is taken from *Müller and Brasseur* [1995]. For methane the deposition velocity varies with temperature and ecosystem type, while for carbon monoxide, it is related to the net primary productivity (NPP). Details are given in Table 6, while Plate 7 shows the geographical distribution of the deposition velocity of ozone for two different seasons. The deposition is expressed as a lower boundary condition in the vertical diffusion equation of the model, and the corresponding loss is therefore independent of the thickness of the lowest layer. A more detailed deposition scheme is currently being developed by coupling MOZART to the land surface model (LSM) of *Bonan* [1996].

7. Spatial and Temporal Variability

The global distributions and budgets of species provided by MOZART will be presented and discussed in the companion paper by *Hauglustaine et al.* [this issue]. However, in order to illustrate the capability of the model to account for spatial and temporal variability associated with meteorological events and to simulate regional pollution episodes, we present and discuss in this section a few specific "snapshots" of the calculated trace gas distributions. Plate 8 shows, for example, an instantaneous global distribution of surface ozone on July 19 at 1200 UT. This figure has to be compared with Plate 12 of *Hauglustaine et al.* [this issue], which shows the monthly average ozone mixing ratio at the surface. Although the two maps show similar patterns, the "snapshot" view shown in Plate 8 exhibits a more irregular structure associated with the specific dynamical situation of the moment. For example, several plumes of ozone originating from the North American continent are visible. In particular, a strong ozone pollution event (50 ppbv) is seen over the Atlantic Ocean in the vicinity of Bermuda. This plume extends east of Canada toward Europe. Export of ozone rich air toward high latitudes is also visible north of the Eurasian continent. Relatively low ozone concentrations are calculated in the continental planetary boundary layer (e.g., South American continent) during nighttime, when dry deposition prevails over photochemistry. High concentrations are found over southern Europe with a local maximum reaching 130 ppbv in Greece.

To provide some insight into the causes of this large ozone concentration seen over the Greek peninsula, we have represented in Figure 8 the day-to-day variation

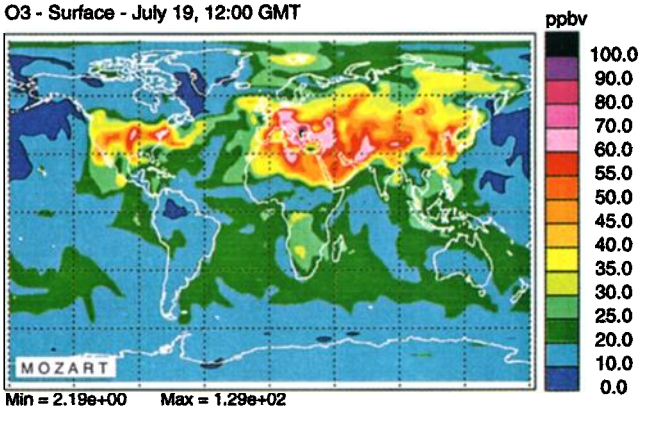

Plate 8. Distribution of ozone mixing ratio (ppbv) calculated at the surface on July 19, 1200 UT.

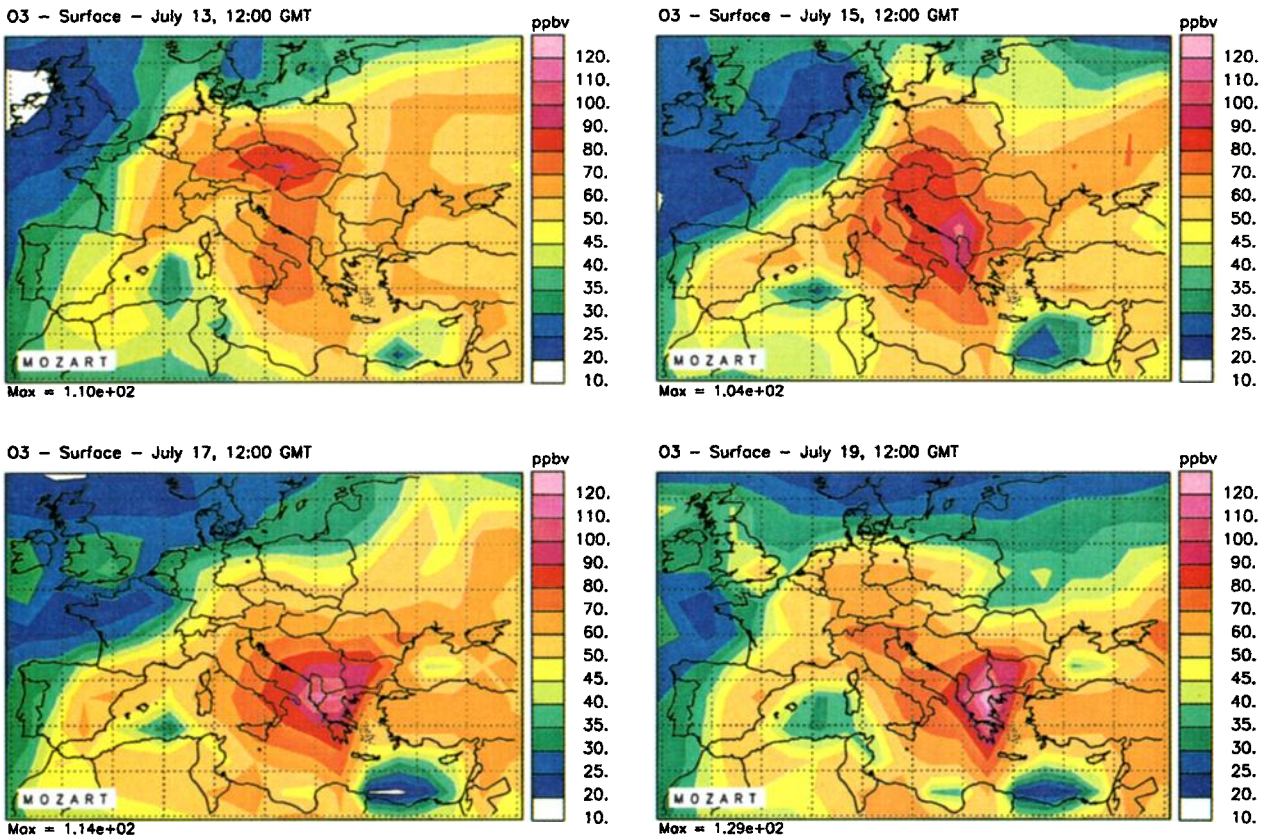

Plate 9. Distribution of ozone mixing ratio (ppbv) calculated at the surface over Europe on July 13, 15, 17, and 19 for midday conditions.

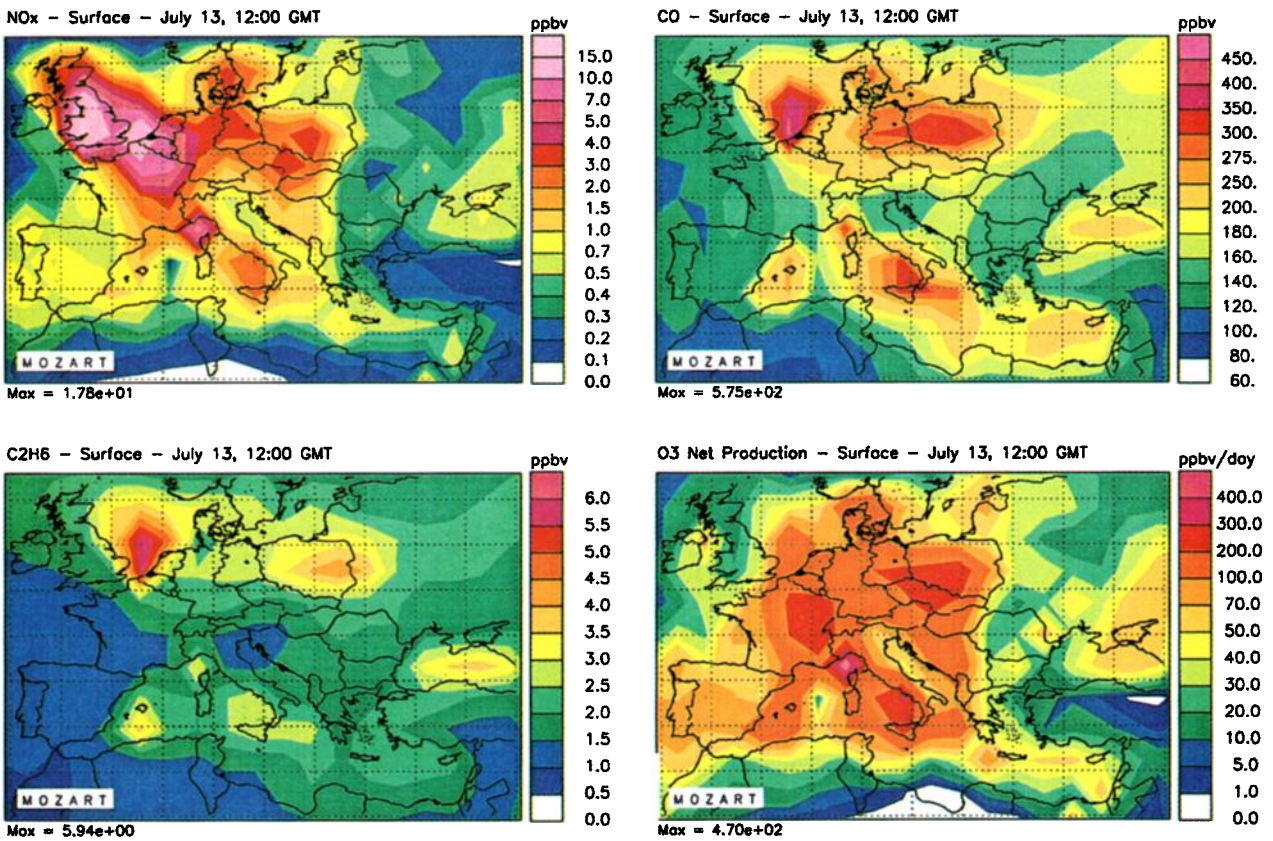

Plate 10. Surface distribution of NO_x, CO, C_2H_6 mixing ratio (ppbv), and O_3 net photochemical production (ppbv/day) calculated over Europe on July 13 for midday conditions.

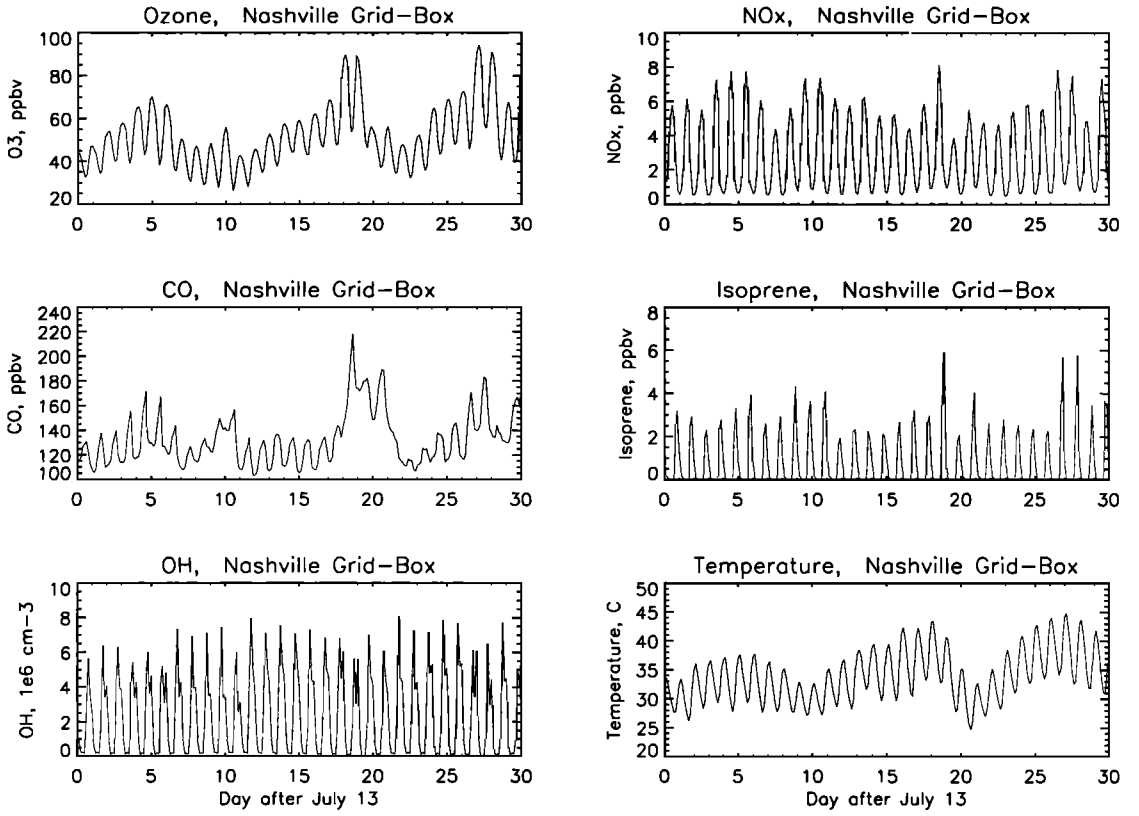

Figure 9. Day-to-day variability of O_3, NO_x, CO, and isoprene mixing ratio (ppbv), OH density ($10^6/cm^3$), and temperature (°C) calculated for the Nashville, TN, grid cell during July 13 and August 13.

of ozone and some of its precursors, as well as of OH, and temperature in the model grid box closest to the city of Athens, from July 13 to August 13. This figure shows substantial diurnal variability for all chemical compounds. In the case of OH the concentration peaks around noon, when photochemical production of radicals is maximum. The daytime maximum of isoprene is related to the diurnal variation in the surface emission of this short-lived biogenic hydrocarbon and reaches 300-1000 pptv at noon. In contrast, the maximum in the concentrations of surface NO_x and CO are found during nighttime, when a local nocturnal inversion develops near the surface, and photochemical losses are small. In the case of ozone the concentration reaches a maximum in the early afternoon as a result of net photochemical production (typically O_3 increases by 15-30 ppbv during the day). The minimum occurring during nighttime results from surface deposition as well as a weak chemical destruction by hydrocarbons. The increasing ozone values seen after July 13 in Athens and reaching a maximum of 110 ppbv on July 19-20 (ozone episode) occurs simultaneously with increasing concentrations of carbon monoxide (350 ppbv on July 18) and of anthropogenic hydrocarbons (not shown). Plates 9a-9d show the evolution of the surface ozone distribution during this period over Europe. The plates illustrate the formation of an ozone episode on July 13 in the eastern part of Germany where the concentrations of NO_x, CO, and anthropogenic NMHCs (Plate 10) are high. In this region the net photochemical production of ozone is higher than over the United Kingdom, for example, where the level of NO_x is sufficiently high to titrate ozone (Plate 10). In the following days the ozone event is displaced toward the southeast by transport of ozone and its precursors in relation to the strong anticyclone over Europe during this period of time. Additional photochemical ozone production along the trajectory of the polluted air masses in the boundary layer explains the increasing concentrations.

Similar ozone episodes are produced by MOZART over the eastern United States. Figure 9, for example, shows the temporal evolution of several chemical compounds over Nashville, TN from July 13 to August 13. In this region of the United States the ozone events are strongly influenced by biogenic hydrocarbons. Two episodes are seen during this period of time, with maximum concentrations larger than 80-90 ppbv during daytime at this site. These events are associated with a doubling in the isoprene mixing ratio (during warm days when biogenic emissions are enhanced) and high values of NO_x and CO. The regional distribution of surface ozone (local noon) calculated by MOZART on August

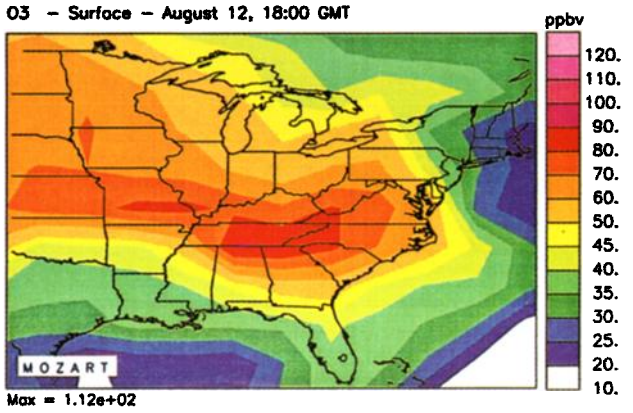

Plate 11. Distribution of ozone mixing ratio (ppbv) calculated at the surface over the southeastern United States on August 12 for midday conditions.

12 (during the second episode) is shown in Plate 11 and is characteristic of observed situations in the southeastern United States during summertime [e.g., Chameides and Cowling, 1995].

8. Conclusions

In this first of two companion papers, we have presented a new chemical transport model of the global troposphere, MOZART, which provides the three-dimensional distribution as well as the global and regional budgets of 56 chemical constituents of the atmosphere. The model, which extends from the surface to the upper stratosphere, has a fairly high horizontal and vertical resolution, and resolves the diurnal cycle with a time step of 20 min. It accounts for surface emissions, large-scale advective and subgrid scale transports, chemical transformations, and wet and dry deposition. One of the specific features of the model is a detailed formulation of vertical exchanges in the planetary boundary layer. The chemical scheme (140 reactions) focuses on the formation and fate of photooxidants, including tropospheric ozone. A discussion of the results provided by the model is presented in a companion paper [*Hauglustaine et al.*, this issue]. Future model developments will include a version of the code driven by assimilated winds and temperature rather than dynamical fields provided by the NCAR CCM. Transport processes will be simulated using a new version of MATCH.

Acknowledgments. The authors are grateful to P. Hess, B. Ridley, L. Horowitz, and J. Orlando for useful comments on this study. They also acknowledge D. Pollard for providing the mass fixer used in MOZART, M. Kritz for making available radon data, J. Caron for developing post-processing and visualization software, and B. Eaton for programming assistance. This work has been supported in part by the National Aeronautics and Space Administration under contracts 2529-MD/BGA-0017 and AEAP-95-014. The National Center for Atmospheric Research is operated by the University Corporation for Atmospheric Research under sponsorship of the National Science Foundation.

References

Andreae, M. O., E. Atlas, H. Cachier, W. R. Cofer III, G. W. Harris, G. Helas, R. Koppmann, J.-P. Lacaux, and D. E. Ward, Trace gas and aerosol emissions from savanna fires, in *Biomass burning and global change*, edited by J. S. Levine, vol. 1, pp. 278-295, MIT press, Mass., 1996.

Atkinson, R., Kinetics and mechanisms of the gas-phase reactions of the hydroxyl radical with organic compounds under atmospheric conditions, *Chem. Rev., 85,* 69-201, 1985.

Atkinson, R., D. L. Baulch, R. A. Cox, R. F. Hampson Jr., J. A. Kerry, and M J. Rossi, Evaluated kinetic and photochemical data for atmospheric chemistry: Supplement V, *Atmos. Environ., 30,* 1996.

Austin, J., N. Butchart, and K. P. Shine, Possibility of an Arctic ozone hole in a doubled-CO_2 climate, *Nature, 360,* 221-225, 1992.

Balkanski, Y. J., D. J. Jacob, and G. M. Gardner, Transport and residence times of tropospheric aerosols inferred from a global three-dimensional simulation of ^{210}Pb, *J. Geophys. Res., 98,* 20,573-20,586, 1993.

Bates, T. S., K. C. Kelly, J. E. Johnson, and R. H. Gammon, Regional and seasonal variations in the flux of oceanic carbon monoxide to the atmosphere, *J. Geophys. Res., 100,* 23,093-23,101, 1995.

Beard, K. V., Terminal velocity and sharps and precipitation drops aloft, *J. Atmos. Sci., 23,* 851-864, 1976.

Benkovitz, C. M., M. T. Scholtz, J. Pacyna, L. Tarrasón, J. Dignon, E. C. Voldner, P. A. Spiro, J. A. Logan, and T. E. Graedel, Global gridded inventories of anthropogenic emissions of sulfur and nitrogen, *J. Geophys. Res., 101,* 29,239-29,253, 1996.

Berntsen, T. K., and I. S. A. Isaksen, A global three-dimensional chemical transport model for the troposphere, 1, Model description and CO and ozone results, *J. Geophys. Res., 102,* 21,239-21,280, 1997.

Best, A. C., The size distribution of raindrops, *Q. J. R. Meteorol. Soc., 76,* 16-36, 1950a.

Best, A. C., Empirical formulae for the terminal velocity of water drops falling through the atmosphere, *Q. J. R. Meteorol. Soc., 76,* 302-311, 1950b.

Bonan, G. B., A land surface model (LSM version 1.0) for ecological, hydrological, and atmospheric studies: Technical description and user's guide, *NCAR Tech. Note, NCAR/TN-417+STR,* Natl. Cent. for Atmos. Res., Boulder, Colo., 1996.

Brasseur, G. P., D. A. Hauglustaine, and S. Walters, Chemical compounds in the remote Pacific troposphere: Comparison between MLOPEX measurements and chemical transport model calculations, *J. Geophys. Res., 101,* 14,795-14,813, 1996.

Brasseur, G. P., X. X. Tie, P. J. Rasch, and F. Lefèvre, A three-dimensional simulation of the Antarctic ozone hole: Impact of anthropogenic chlorine on the lower stratosphere and upper troposphere, *J. Geophys. Res., 102,* 8909-8930, 1997.

Burden, R. L., and J. D. Faires, *Numerical Analysis*, PWS, Boston, Mass., 1985.

Cantrell, C. A., W. R. Stockwell, L. G. Anderson, K. L. Busarow, D. Perner, A. Schmeltekopf, J. G. Calvert, and H. S. Johnston, Kinetic study of the NO_3-CH_2O reaction and its possible role in nighttime tropospheric chemistry, *J. Phys. Chem., 89,* 139-146, 1985.

Carter, W. P. L., A detailed mechanism for the gas-phase atmospheric reactions of organic compounds, *Atmos. Environ., 24,* 481-518, 1990.

Chameides, W. L., and E. B. Cowling, *The State of the Southern Oxidants Study (SOS): Policy-Relevant Find-*

ings in Ozone Pollution Research 1988-1994, Southern Oxidant Study, Coll. of Forest Resour., N. C. State Univ., Raleigh, 1995.

Chang, J. S., R. A. Brost, I. S. A. Isaksen, S. Madronich, P. Middleton, W. R. Stockwell, and C. J. Walcek, A three-dimensional Eulerian acid deposition model: Physical concepts and formulation, *J. Geophys. Res., 92,* 14,681-14,700, 1987.

Chin, M., D. J. Jacob, G. M. Gardner, M. S. Foreman-Folwer, and P. A. Spiro, A global three-dimensional model of tropospheric sulfate, *J. Geophys. Res., 101,* 18,667-18,690, 1996.

Chipperfield, M. P., D. Cariolle, P. Simon, R. Ramaroson, and D. J. Lary, A three-dimensional modeling study of trace species in the Arctic lower stratosphere during winter 1989-1990, *J. Geophys. Res., 98,* 7199-7218, 1993.

Chipperfield, M. P., D. Cariolle, and P. Simon, A 3D chemical transport model study of chlorine activation during EASOE, *Geophys. Res. Lett., 21,* 1467-1470, 1994.

Chipperfield, M. P., J. A. Pyle, C. E. Blom, N. Glatthor, M. Höpfner, T. Gulde, C. Piesch, and P. Simon, The variability of $ClONO_2$ and HNO_3 in the Arctic polar vortex: Comparison of Traansall Michelson interferometer for passive atmospheric sounding measurements and three-dimensional model results, *J. Geophys. Res., 100,* 9115-9129, 1995.

Crutzen, P. J., and P. H. Zimmermann, The changing photochemistry of the troposphere, *Tellus, 43,* 136-151, 1991.

Cunnold, D. M., P. J. Fraser, R. F. Weiss, R. G. Prinn, P. G. Simmonds, F. N. Alyea, and A. J. Crawford, Global trends and annual releases of $CFCl_3$ and CF_2Cl_2 estimated from ALE/GAGE and other measurements from July 1978 to June 1991, *J. Geophys. Res., 99,* 1107-1126, 1994.

DeMore, W. B., S. P. Sander, D. M. Golden, R. F. Hampson, M. J. Kurylo, C. J. Howard, A. R. Ravishankara, C. E. Kolb, and M. J. Molina, *Chemical Kinetics and Photochemical Data for Use in Stratospheric Modeling, JPL Publ. 97-4,* Jet Propul. Lab., Pasadena, Calif., 1997.

Dentener, F. J., and P. J. Crutzen, A three-dimensional model of the global ammonia cycle, *J. Atmos. Chem., 19,* 331-369, 1994.

Dentener, F. J., G. R. Carmichael, Y. Zhang, J. Lelieveld, and P. J. Crutzen, Role of mineral aerosol as a reactive surface in the global troposphere, *J. Geophys. Res., 101,* 22,869-22,889, 1996.

Emmons, L. K., et al., Climatologies of NO_x and NO_y: A comparison of data and models, *Atmos. Environ., 31,* 1851-1904, 1997.

Erickson, D. J., III, and J. A. Taylor, 3-D tropospheric CO modeling: The possible influence of the ocean, *Geophys. Res. Lett., 19,* 1955-1958, 1992.

Feichter, J., and P. J. Crutzen, Parameterization of vertical tracer transport due to deep cumulus convection in a global transport model and its evaluation with ^{222}radon measurements, *Tellus, Ser. B, 42,* 100-117, 1990.

Fenton, D. L., R. Y. Purcell, and D. Hrdina, The washout of combustion-generated hydrogen chlorine, *Atmos. Environ., 14,* 1055-1062, 1980.

Friedl, R. (Ed.), Atmospheric effects of subsonic aircraft: Interim assessment report of the advanced subsonic technology program, *NASA Ref. Publ. 1400,* 143 pp., 1997.

Frossling, N., The evaporating of falling drops, *Beitr. Geophys., 52,* 170-216, 1938.

Fung, I., K. Prentice, E. Matthews, J. Lerner, and G. Russel, Three-dimensional tracer model study of atmospheric CO_2: Response to seasonal exchanges with the terrestrial biosphere, *J. Geophys. Res., 88,* 1281-1294, 1983.

Fung I., J. John, J. Lerner, E. Matthews, M. J. Prather, L. P. Steele, and P. J. Fraser, Global budgets of atmospheric methane: Results from a three-dimensional global model synthesis, *J. Geophys. Res., 96,* 13,033-13,065, 1991.

Gierczak, T., J. B. Burkholder, S. Bauerle, and A. R. Ravishankara, Laboratory study of the photolysis of acetone in air, *J. Atmos. Chem.,* in press, 1998.

Giorgi, F., and W. L. Chameides, The rainout parameterization in a photochemical model, *J. Geophys. Res., 90,* 7872-7880, 1985.

Granier, C., and G. Brasseur, Impact of heterogeneous chemistry on model predictions of ozone changes, *J. Geophys. Res., 97,* 18,015-18,033, 1992.

Granier, C., W. M. Hao, G. Brasseur, and J.-F. Müller, Land use practices and biomass burning: Impact on the chemical composition of the atmosphere, in *Biomass Burning and Global Change,* edited J. S. Levine, pp. 140-198, MIT Press, Cambridges, Mass., 1996.

Grose, W. L., J. E. Nealy, R. E. Turner, and W. T. Blackshear, Modeling the transport of chemically active constituents in the stratosphere, in *Transport Processes in the Middle Atmosphere,* edited by G. Visconti, and R. Garcia, pp. 229-250, D. Reidel, Norwell, Mass., 1987.

Hack, J. J., Parameterization of moist convection in the NCAR community climate model (CCM2), *J. Geophys. Res., 99,* 5551-5568, 1994.

Hack, J. J., and J. T. Kiehl, Reduction of systematic errors in the NCAR CCM2, *WCRP-92 WMO/TD 732,* pp. 313-318, World Meteorol. Organ., Geneva, 1995.

Hack, J. J., B. A. Boville, B. P. Briegleb, J. T. Kiehl, P. J. Rasch, and D. L. Williamson, Description of the NCAR Community Climate Model (CCM2), *NCAR Tech. Note NCAR/TN-382+STR,* Natl. Cent. for Atmos. Res., Boulder, Colo., 1993.

Hack, J. J., B. A. Boville, J. T. Kiehl, P. J. Rasch, and D. L. Williamson, Climate statistics from the National Center for Atmospheric Research community climate model CCM2, *J. Geophys. Res., 99,* 20,785-20,813, 1994.

Hall, I. W., R. P. Wayne, R. A. Cox, M. E. Jenkin, and G. D. Hayman, Kinetics of the reaction of NO_3 with HO_2, *Int. J. Phys. Chem., 92,* 5049-5054, 1988.

Hao, W. M., and M.-H. Liu, Spatial distribution of tropical biomass burning in 1980 with 5° × 5° resolution, *Global Biogeochem. Cycles, 8,* 495-503, 1994.

Hao, W. M., D. E. Ward, G. Olbu, and S. P. Baker, Emissions of CO_2, CO, and hydrocarbons from fires in diverse African savanna ecosystems, *J. Geophys. Res., 101,* 23,577-23,584, 1996.

Hartley, D. E., D. L. Williamson, P. J. Rasch, and R. G. Prinn, Examination of tracer transport in the NCAR CCM2 by comparison of $CFCl_3$ simulations with ALE/GAGE observations, *J. Geophys. Res., 99,* 12,885-12,896, 1994.

Hauglustaine, D. A., B. A. Ridley, S. Solomon, P. G. Hess, and S. Madronich, HNO_3/NO_x ratio in the remote troposphere during MLOPEX 2: Evidence for nitric acid reduction on carbonaceous aerosols? *Geophys. Res. Lett., 23,* 2609-2612, 1996.

Hauglustaine, D. A., G. P. Brasseur, and S. Walters, A Three-Dimensional Simulation of Ozone over the North Atlantic Ocean, in *Atmospheric Ozone,* R. D. Bojkov and G. Visconti (Eds), pp. 735-738, International Ozone Commission, L'Aquila, 1998.

Hauglustaine, D. A., G. P. Brasseur, S. Walters, P. J. Rasch, J.-F. Müller, L. K. Emmons, and M. A. Carroll, MOZART, a global chemical transport model for ozone and related chemical tracers, 2, Model results and evaluation, *J. Geophys. Res.,* this issue.

Hesstvedt, E., Ö. Høv, and I. S. A. Isaksen, Quasi-steady-state approximations in air pollution modeling: Compari-

son of two numerical schemes for oxidant prediction, *Intl. J. Chem. Kinetics, X,* 971-994, 1978.

Holtslag, A., and B. Boville, Local versus nonlocal boundary-layer diffusion in a global climate model, *J. Clim., 6,* 1825-1842, 1993.

Hurrell, J. W., Comparison of NCAR community climate model (CCM) climates, *Clim. Dyn., 11,* 25-50, 1995.

Jacob, D. J., M. J. Prather, S. C. Wofsy, and M. B. McElroy, Atmospheric distribution of ^{85}Kr simulated with a general circulation model, *J. Geophys. Res., 92,* 6614-6626, 1987.

Jacob, D. J., and M. J. Prather, Radon-222 as a test of convective transport in a general circulation model, *Tellus, Ser. B, 42,* 118-134, 1990.

Jacob, D. J., et al., Simulation of summertime ozone over North America, *J. Geophys. Res., 98,* 14,797-14,816, 1993.

Jacob, D. J., et al., Evaluation and intercomparison of global atmospheric transport models using ^{222}Rn and other short-lived tracers, *J. Geophys. Res., 102,* 5953-5970, 1997.

Jaeglé, L., et al., Observed OH and HO_2 in the upper troposphere suggest a major source from convective injection of peroxides, *Geophys. Res. Leit., 24,* 3181-3184, 1997.

Kanakidou, M., and P. J. Crutzen, Scale problems in global tropospheric chemistry modeling: Comparison of results obtained with a three-dimensional model, adopting longitudinally uniform and varying emissions of NO_x and NMHC, *Chemosphere, 26,* 787-802, 1993.

Kanakidou, M., H. B. Singh, K. M. Valentin, and P. J. Crutzen, A two-dimensional study of ethane and propane oxidation in the troposphere, *J. Geophys. Res., 96,* 15,395-15,413, 1991.

Kasibhatla, P., H. Levy II, and W. J. Moxim, Global NO_x, HNO_3, PAN, and NO_y distributions from fossil fuel combustion emissions: A model study, *J. Geophys. Res., 98,* 7165-7180, 1993.

Kasibhatla, P., H. Levy II, A. Klonecki, and W. L. Chameides, Three-dimensional view of the large-scale tropospheric ozone distribution over the North Atlantic Ocean during summer, *J. Geophys. Res., 101,* 29,305-29,316, 1996.

Kiehl, J. T., J. J. Hack, G. Bonan, B. Briegleb, D. L. Williamson, and P. J. Rasch, Description of the NCAR Community Climate Model (CCM3), *NCAR/TN-420+STR,* Natl Cent. for Atmos. Res., Boulder, Colo., 1996.

Kiehl, J. T., J. J. Hack, G. B. Bonan, B. B. Boville, D. L. Williamson, and P. J. Rasch, The National Center for Atmospheric Research Community Climate Model: CCM3, *J. Clim., 11,* 1131-1149, 1998.

Kraus, A. B., F. Rohrer, E. S. Grobler, and D. H. Ehhalt, The global tropospheric distribution of NO_x estimated by a three-dimensional chemical tracer model, *J. Geophys. Res., 101,* 18,587-18,604, 1996.

Lary, D. J., A. M. Lee, R. Toumi, M. J. Newchurch, M. Pirre, and J. B. Renard, Carbon aerosols and atmospheric photochemistry, *J. Geophys. Res., 102,* 3671-3682, 1997.

Lee, H. N., and J. Feichter, An intercomparison of wet precipitation scavenging schemes and the emission rates of ^{222}Rn for the simulation of global transport and deposition of ^{210}Pb, *J. Geophys. Res., 100,* 23,253-23,270, 1995.

Lefèvre, F., G. P. Brasseur, I. Folkins, A. K. Smith, and P. Simon, Chemistry of the 1991-1992 stratospheric winter: Three-dimensional model simulations, *J. Geophys. Res., 99,* 8183-8195, 1994.

Le Texier, H., S. Solomon, and R. R. Garcia, The role of molecular hydrogen and methane oxidation in the water vapor budget of the stratosphere, *Q. J. R. Meteorol. Soc., 114,* 281-295, 1988.

Levine, S. Z., and S. E. Schwarz, In-cloud and below-cloud scavenging of acid vapor, *Atmos. Environ., 16,* 1725-1734, 1982.

Levy, H., II, J. D. Mahlman, and W. J. Moxim, Tropospheric N_2O variability, *J. Geophys. Res., 87,* 3061-3080, 1982.

Levy, H., II, J. D. Mahlman, and W. J. Moxim, Tropospheric ozone: The role of transport, *J. Geophys. Res., 90,* 3753-3772, 1985.

Liu, S. C., J. R. McAfee, and R. J. Cicerone, $^{222}Radon$ and tropospheric vertical transport, *J. Geophys. Res., 89,* 7291-7297, 1984.

Madronich, S., and J. G. Calvert, The NCAR master mechanism of the gas phase chemistry-Version 2.0, NCAR Tech. Note NCAR/TN-333+STR, Natl Cent. for Atmos. Res., Boulder, Colo., 1989.

Mahlman, J. D., and W. J. Moxim, Tracer simulation using a global general circulation model: Results from a midlatitude instantaneous source experiment, *J. Atmos. Sci., 35,* 1340-1374, 1978.

Mahowald, N. M., Development of a 3-dimensional chemical transport model based on observed winds and use in inverse modeling of the sources of CCl_3F, Ph.D. thesis, MIT, Cambridge, Mass., 1996.

Mahowald, N. M., P. J. Rasch, and R. G. Prinn, Cumulus parameterization in chemical transport models, *J. Geophys. Res., 100,* 26,173-26,189, 1995.

Mahowald, N. M., R. G. Prinn, and P. J. Rasch, Deducing CCl_3F emissions using an inverse method and chemical transport models with assimilated winds, *J. Geophys. Res., 102,* 28,153-28,168, 1997a.

Mahowald, N. M., P. J. Rasch, B. E. Eaton, S. Whittlestone, and R. G. Prinn, Transport of $^{222}Radon$ to the remote troposphere using MATCH and assimilated winds from ECMWF and NCEP/NCAR, *J. Geophys. Res., 102,* 28,139-28,152, 1997b.

Moortgat, G. K., B. Veyret, and R. Lesclaux, Kinetics of the reaction of HO_2 with $CH_3C(O)O_2$ in the temperature range 253-368 K, *Chem. Phys. Lett., 160,* 443-447, 1989.

Müller, J.-F., Geographical distribution and seasonal variation of surface emissions and deposition velocities of atmospheric trace gases, *J. Geophys. Res., 97,* 3787-3804, 1992.

Müller, J.-F., and G. Brasseur, IMAGES: A three-dimensional chemical transport model of the global troposphere, *J. Geophys. Res., 100,* 16,445-16,490, 1995.

Nevison, C., A model analysis of the spatial distribution and temporal trends of nitrous oxide sources and sinks, Ph.D. thesis, Stanford Univ., Stanford, Calif., 1994.

Penner, J. E., C. S. Atherton, J. Dignon, S. J. Ghan, J. J. Walton, S, Hameed, Tropospheric nitrogen: a three-dimensional study of sources, distributions, and deposition, *J. Geophys. Res., 96,* 959-990, 1991.

Pham, M., J.-F. Müller, G. P. Brasseur, C. Granier, and G. Mégie, A three-dimensional study of the tropospheric sulfur cycle, *J. Geophys. Res., 100,* 26,061-26,092, 1995.

Prather, M. J., M. B. McElroy, S. C. Wofsy, G. Russel, and D. Rind, Chemistry of the global troposphere: Fluorocarbons as tracers of air motion, *J. Geophys. Res., 92,* 6579-6613, 1987.

Price, C., and D. Rind, A simple lightning parameterization for calculating global lightning distributions, *J. Geophys. Res., 97,* 9919-9933, 1992.

Rasch, P. J., and J. E. Kristjansson, A comparison of the CCM3 model climate using diagnosed and predicted condensate parameterizations, *J. Clim.,* in press, 1998.

Rasch, P. J., and M. Lawrence, Recent developments in transport methods at NCAR, in *Proceedings of the 1997 Workshop on transport methods,* Max Planck Inst. for, Meteorol., Hamburg, Germany, in press, 1998.

Rasch, P. J., and D. L. Williamson, Computational aspects of moisture transport in global models of the atmosphere, *Q. J. R. Meteorol. Soc., 116,* 1071-1090, 1990.

Rasch, P. J., X. X. Tie, B. A. Boville, and D. L. Williamson, A three-dimensional transport model for the middle atmosphere, *J. Geophys. Res., 99,* 999-1017, 1994.

Rasch, P. J., B. A. Boville, and G. P. Brasseur, A three-dimensional general circulation model with coupled chemistry for the middle atmosphere, *J. Geophys. Res., 100,* 9041-9071, 1995.

Rasch, P. J., N. M. Mahowald, and B. E. Eaton, Representations of transport, convection and the hydrologic cycle in chemical transport models: Implications for the modeling of short lived and soluble species, *J. Geophys. Res., 102,* 28,127-28,138, 1997.

Rehfeld, S., and M. Heimann, Three dimensional atmospheric transport simulation of the radioactive tracers ^{210}Pb, ^{7}Be, ^{10}Be, and ^{90}Sr, *J. Geophys. Res., 100,* 26,141-26,161, 1995.

Richtmyer, R. D., and K. W. Morton, *Difference Methods for Initial-Value Problems,* Wiley-Interscience, New York, 1967.

Roelofs, G.-J., and J. Lelieveld, Distribution and budget of O_3 in the troposphere calculated with a chemistry general circulation model, *J. Geophys. Res., 100,* 20,983-20,998, 1995.

Rose, K., and G. Brasseur, A three-dimensional model of chemically active trace species in the middle atmosphere during disturbed winter conditions, *J. Geophys. Res., 94,* 16,387-16,403, 1989.

Sandu, A., J. G. Verwer, J. G. Blom, E. J. Spee, and G. R. Carmichael, Benchmarking stiff ODE solvers for atmospheric chemistry problems II: Rosenbrock solvers, *Rep. Comput. Math., 90/1996,* Univ. of Iowa, Ames, 1996.

Simmons, A. J., and R. Strüfing, An energy and angular-momentum conserving finite-difference scheme, hybrid coordinates and medium-range weather prediction, *ECMWF Tech. Rep. 28,* 68 pp., Eur. Cent. for Medium-Range Weather Forecasts, Reading, England, 1981.

Singh, H. B., M. Kanakidou, P. J. Crutzen, and D. J. Jacob, High concentrations and photochemical fate of oxygenated hydrocarbons in the global troposphere, *Nature, 378,* 50-54, 1995.

Slingo, A., A GCM parameterization for the shortwave radiative properties of water clouds, *J. Atmos. Sci., 46,* 1419-1427, 1989.

Taylor, J. A., G. P. Brasseur, P. R. Zimmerman, and R. J. Cicerone, A study of the sources and sinks of methane and methyl chloroform using a global three-dimensional Lagrangian tropospheric tracer transport model, *J. Geophys. Res., 96,* 3013-3044, 1991.

Tie, X. X., and P. Hess, Ozone mass exchange between the stratosphere and troposphere for background and volcanic sulfate aerosol conditions, *J. Geophys. Res., 102,* 25,487-25,500, 1997.

Williamson, D. L., and P. J. Rasch, Two-dimensional semi-Lagrangian transport with shape preserving interpolation, *Mon. Weather Rev., 117,* 102-129, 1989.

World Meteorological Organization, Scientific assessment of ozone depletion: 1991, *WMO Rep. 25,* World, Geneva, 1991.

Zimmerman, J., and D. Poppe, A supplement for the RADM2 chemical mechanism: The photooxidation of isoprene, *Atmos. Environ., 30,* 1255-1269, 1996.

G. P. Brasseur, P. J. Rasch, X. X. Tie, and S. Walters, National Center for Atmospheric Research, P. O. Box 3000, Boulder, CO 80307-3000.

C. Granier and D. A. Hauglustaine, Service d'Aéronomie du CNRS, Université de Paris 6, 4, place Jussieu, F-75252 Paris CEDEX 05, France. (dh@aero.jussieu.fr)

J.-F. Müller, Belgian Institute for Space Aeronomy, 3 avenue circulaire, B-1180 Brussels, Belgium.

(Received February 20, 1998; revised July 7, 1998; accepted July 9, 1998.)